

# ISM Abundances in Sculptor Group Dwarf Irregular Galaxies

Evan D. Skillman<sup>1</sup>

*Astronomy Department, University of Minnesota, Minneapolis, MN 55455*

[skillman@astro.umn.edu](mailto:skillman@astro.umn.edu)

Stéphanie Côté

*Canadian Gemini Office, HIA/NRC of Canada, 5071 West Saanich Rd., Victoria, B.C., Canada,  
V9E 2E7*

[Stephanie.Cote@hia.nrc.ca](mailto:Stephanie.Cote@hia.nrc.ca)

and

Bryan W. Miller

*AURA/Gemini Observatory, Casilla 603, La Serena, Chile;*

[bmiller@gemini.edu](mailto:bmiller@gemini.edu)

## ABSTRACT

Using the CTIO 4-m telescope, we have obtained optical spectra of HII regions in five Sculptor Group dwarf irregular galaxies. We derive oxygen, nitrogen, and sulfur abundances from the HII region spectra. Oxygen abundances are derived via three different methods (the “direct” method, the empirical method guided by photoionization modeling of McGaugh (1991), and the purely empirical method of Pilyugin (2000)) and are compared. Significant systematic differences are found between the three methods, and we suggest that a recalibration of the empirical abundance scale is required. Until differences between these three methods are better understood, the issue of the degree of uniformity of the ISM abundances in a dwarf galaxy cannot be properly addressed. The N/O ratio for the metal-poor dI ESO 473-G24 of  $\log (N/O) = -1.43 \pm 0.03$  lies well above the plateau of  $\log (N/O) = -1.60 \pm 0.02$  found by Izotov & Thuan (1999) for a collection of metal-poor blue compact galaxies. This shows that not all galaxies with  $12 + \log (O/H) \leq 7.6$  have identical elemental abundance ratios, and this implies that the Izotov & Thuan scenario for low metallicity galaxies is not universal.

---

<sup>1</sup>Visiting Astronomer, Cerro Tololo Inter-American Observatory, National Optical Astronomy Observatory, which is operated by the Association of Universities for Research in Astronomy, Inc. (AURA) under cooperative agreement with the National Science Foundation.

Measurements of the HII regions in NGC 625 yield  $\log (N/O) \approx -1.25$ . Assuming N production by intermediate mass stars, this relatively high N/O ratio may be indicative of a long quiescent period prior to the recent active burst of star formation. The oxygen abundances in the Sculptor Group dIs are in good agreement with the relationship between metallicity and luminosity observed in the Local Group dIs. Taken together the observations show a better relationship between metallicity and luminosity than between metallicity and galaxy central surface brightness. The Sculptor Group dIs, in general, lie closer to the simple closed box model evolutionary path than the Local Group dIs. The higher gas contents, lower average star formation rates, and closer resemblance to closed box evolution could all be indicative of evolution in a relatively low density environment.

*Subject headings:* galaxies: abundances — galaxies: individual (NGC 625) — galaxies: irregular — galaxies: evolution — HII regions

## 1. Introduction

Low-mass dwarf irregular galaxies provide an important testing ground for several fundamental questions about star formation, galactic evolution, and cosmology. Due, in large part, to attempts to understand the possible evolutionary connections between the dwarfs with negligible or extremely low present star formation rates (the dSph and dE galaxies, hereafter dE galaxies) and the dwarfs with obvious signs of present star formation (the dIrrs, blue compact dwarfs, HII galaxies, hereafter dI galaxies), many theorists are turning their attention to the problem of dwarf galaxy evolution (see introduction to Skillman, Côté, & Miller 2002; hereafter paper 1). By comparing the properties of dwarf galaxies in different environments we may be able to isolate key environmental variables (e.g., local density, companionship, group vs. cluster membership) in order to constrain these theories.

Dwarf irregular galaxies generally show low metallicities, (see e.g., Skillman et al. 1989a,b), and thus, are ideal laboratories for studying the early stages of nucleosynthesis in galaxies and constraining the primordial He abundance in the early universe (see e.g., Lequeux et al. 1979; Pagel et al. 1992). It is generally found that the metallicity of the ISM of dIs correlates very well with the galaxy's luminosity (Lequeux et al. 1979; Talent 1980; Kinman & Davidson 1981; Skillman, Kennicutt, & Hodge 1989; Richer & McCall 1995; van Zee et al. 1997b), but some studies do not support this (e.g., Hidalgo-Gamez & Olofsson 1998; Hunter & Hoffman 1999; but see also Pilyugin 2001). Various explanations of the physical basis for the metallicity – luminosity relationship exist, and the simplest are those based on the idea that dwarf galaxies of decreasing mass are less likely to retain the recently synthesized heavy elements returned to the ISM by type II supernovae (e.g., Larson 1974; Dekel & Silk 1986; but see also Skillman 1997).

It may be possible to identify the physical process(es) underlying the metallicity – luminosity relationship by examining galaxies with extreme properties (e.g., Kennicutt & Skillman 2001). With

that goal in mind, the motivation for this study was to measure the ISM abundances in nearby groups of galaxies in order to compare with the galaxies from the Local Group. By comparing galaxies in different environments, it may be possible to determine environmental effects on the metallicity – luminosity relationship. For example, Skillman et al. (1996) discovered that stripped spiral galaxies in the core of the Virgo cluster showed elevated ISM abundances and Vílchez (1995) showed evidence for elevated abundances in the dwarf galaxies associated with the Virgo cluster.

Studies of the relative abundances of nitrogen and oxygen in dwarf irregular galaxies potentially provide an independent measurement of recent average star formation rates. From a study of the Pegasus dI, Skillman, Bomans, & Kobulnicky (1997) found an unusually high N/O ratio which is interpreted as due to a quiescent star formation history over the last few 100 million years. This is in line with the paucity of HII regions, the red color, and the recent star formation history derived from HST stellar photometry (Gallagher et al. 1998). This demonstrates that, in some cases, the N/O abundance can be used as a measure of the relative star formation rate over the last few 100 million years (Kobulnicky & Skillman 1998). Skillman et al. (1997) argue that measuring N/O in a sample of dIs with a large range in colors may allow us to calibrate the time delay of the N delivery (from intermediate mass stars) relative to the O delivery (from massive stars). This is an important parameter for the interpretation of the abundances of the damped Lyman- $\alpha$  systems (Pettini et al. 1995; Lu et al. 1998). Much of the work in this field has concentrated on the high surface brightness HII galaxies, but there is suspicion of chemical “self pollution” of the emission line region by the current burst of star formation (Kunth & Sargent 1986; but see also discussions in Skillman & Kennicutt 1993, Kobulnicky & Skillman 1996, 1997). This may be less of a concern for the more modest HII regions which can be observed in nearby dI galaxies; these systems are not powered by the giant superclusters seen in more distant galaxies, and so their chemical environments may be more pristine. The low present star formation rates observed in the Sculptor group dwarfs make them ideal objects for testing the N/O “clock”.

The Sculptor group is the closest group of galaxies beyond our Local Group. Its properties are reviewed in paper 1 and references in that paper. In paper 1 we presented new H $\alpha$  imaging of a sample of Sculptor Group dIs. HII regions were detected in eight dwarf irregular galaxies. Here we have used the CTIO 4-m to obtain optical spectra of ten HII regions located in five of these dwarf irregular galaxies. These spectra are used to measure chemical abundances, which are compared to the HII region chemical abundances available for Local Group dIs.

## 2. Spectrophotometric Observations

Spectra were taken with the cassegrain R-C spectrograph ( $f/7.8$ ) on the CTIO 4-m telescope on the evening of 6 September 1997 and the first half of 7 September 1997. High humidity and precipitation prevented observations on the second half of 7 September 1997 and 8 September 1997. We used the Blue Air Schmidt camera with a Loral thinned 3K  $\times$  1K format CCD with 15  $\mu$  pixels as the detector. A 527 line mm $^{-1}$  grating (KPGL3) resulted in a dispersion scale of 1.91  $\text{\AA}$  pixel $^{-1}$

and a spatial scale of  $0.50''/\text{pixel}^{-1}$ . A uv (WG360;  $3600\text{ \AA}$ ) blocking filter was used to suppress second order contamination in the red. Useful data were collected over the wavelength range of  $3600 - 7100\text{ \AA}$ . Observations were obtained with a  $1.3''$  wide slit observing at low air mass and near the parallactic angle in order to avoid problems of differential atmospheric refraction (cf. Filippenko 1982). The projected slit length is slightly larger than  $3'$ .

Bias frames, dome flats, twilight sky flats, and He-Ne-Ar comparison exposures were taken at the beginning and end of the nights. On the first night, three standard stars from the list of Oke (1990) were observed ( $2 \times$  LTT 9491,  $2 \times$  Feige 110, G158-100). LTT 9491 and Feige 110 were observed on the second night. The standard stars were observed with a slit width of  $6''$  in order to avoid any effects of differential atmospheric refraction.

Observations of a total of ten HII regions in five different galaxies were obtained as follows:  $2 \times 1800\text{s}$  observations were made of E347-G17 #5 & #10 (see paper 1) at an average airmass of 1.2 with an E-W slit position angle,  $3 \times 1800\text{s}$  observations were made of E348-G09 #3 (paper 1) at an average airmass of 1.1 with an E-W slit position angle,  $4 \times 1200\text{s}$  observations were made of E471-G06 #2 (as numbered by Miller 1996) at an average airmass of 1.4 with an E-W slit position angle,  $4 \times 1800\text{s}$  observations were made of E473-G24 #2 & #4 (paper 1) at an average airmass of 1.02 with an E-W slit position angle, and  $3 \times 1800\text{s}$  observations were made of NGC 625 #5, #9, #18, and #21 (paper 1) at an average airmass of 1.06 with a position angle of  $-98^\circ$ .

Standard reduction procedures were followed using the programs available within the IRAF<sup>2</sup> system. The standard star observations from the two nights were reduced independently and compared. Because no systematic differences could be detected, both night's data were combined and analyzed together (i.e., using the same sensitivity function and the same extinction law). Because G158-100 is a relatively red star (spectral type sdG) the variation between its sensitivity calibration and the other two bluer stars indicated at what wavelength the spectra of the blue stars were beginning to be affected by second order contamination ( $\sim 6860\text{ \AA}$ , although the atmospheric “B” band due to  $\text{O}_2$  absorption confuses the precise onset of the effect). Note that second order contamination is found well before the  $\lambda 7200$  that one derives by simply doubling the  $\lambda 3600$  wavelength of the second-order blocking filter. This is simply because the  $\lambda 3600$  refers to the 50% point of the filter, and the profile of the transmission of the filter is far from step-like. Beyond this wavelength only G158-100 was used for determining the sensitivity curve (the flux of G158-100 is roughly 2 magnitudes weaker at  $\lambda 3500$  compared to  $\lambda 7000$ , so this should provide a good calibration out to the red limit of our observations at  $\sim \lambda 7100$ ). This means that for emission lines between  $\sim 6860\text{ \AA}$  and  $\sim \lambda 7100\text{ \AA}$ , the fluxes of the emission lines should not be affected, but that the continuum of the HII region targets may be contaminated by second order light (thus reducing the emission line equivalent widths). In principle, this is only important for using the [He I]  $\lambda 7065$  line to derive a helium abundance if corrections for underlying absorption are applied on an equivalent width basis.

---

<sup>2</sup>IRAF is distributed by the National Optical Astronomy Observatories, which are operated by the Association of Universities for Research in Astronomy, Inc., under cooperative agreement with the National Science Foundation.

Because the standard stars were observed over a large range in airmass, during the flux calibration stage, an extinction law could be derived from the standard star data. This agreed to within a few percent with the extinction law derived for the CTIO observatory and supplied within IRAF.

Extracted spectra are shown for the brightest HII region in each of the five galaxies in Figures 1a-e. Emission lines were identified, and fluxes and errors were measured following the method of Skillman & Kennicutt (1993; SK93). Values of the logarithmic extinction at  $H\beta$ ,  $C(H\beta)$ , were derived from the error weighted average of determinations from the  $H\alpha/H\beta$ ,  $H\gamma/H\beta$ , and  $H\delta/H\beta$  ratios while simultaneously solving for the effects of underlying stellar absorption,  $EW(HI-abs)$ , (assumed to be equal in equivalent width for all four Balmer lines). We assumed the intrinsic case B Balmer line ratios calculated by Hummer & Storey (1987), and used the reddening law of Seaton (1979) as parameterized by Howarth (1983), assuming a value of  $R = A_V/E_{B-V} = 3.2$ . The assumed reddening law has no associated uncertainty. Uncertainties in  $C(H\beta)$  and  $EW(HI-abs)$  were determined from Monte Carlo simulations (Olive & Skillman 2001). Figure 2 shows an example solution for one of the observed HII regions. Note that the errors derived in this way are often significantly larger than those derived in the literature by either assuming a value for the underlying absorption or derived from a  $\chi^2$  analysis without a Monte Carlo analysis of the errors. When the Balmer lines were corrected for underlying absorption, the higher numbered Balmer lines ( $H9$ ,  $H10$ ,  $H11$ , and  $H12$ ) were not assumed to have identical values in terms of equivalent width, but were assumed to have values of 0.80, 0.65, 0.50, and 0.40 respectively of the lower numbered Balmer lines, guided by the low metallicity, instantaneous burst models of González-Delgado, Leitherer, & Heckman (1999). Note that all of the Sculptor Group dIs lie at Galactic latitudes more negative than  $-69^\circ$ , and thus, Galactic extinction along the lines of sight to the H II regions should be negligible (e.g., the Galactic foreground  $E(B-V)$  for the Sculptor dwarf irregular galaxy, which lies near the middle of the projected distribution, is calculated to be 0.012 mag by Schlegel et al. 1998). The corrected fluxes for the ten HII region spectra, relative to  $H\beta$ , are listed in Table 1.

### 3. The Chemical Abundances in Five Sculptor Group Dwarf Irregular Galaxies

#### 3.1. The Oxygen Abundance

Oxygen abundances are derived for the HII regions by three different methods: the “direct” method (cf. Dinerstein 1990, Skillman 1998), the empirical method of McGaugh (1991), which is guided by the use of photoionization models, and the purely empirical method of Pilyugin (2000). A reliable measurement of the electron temperature of the ionized gas is necessary for the “direct” conversion of emission line strengths into ionic abundances. In most cases of metal poor HII regions, this is done by measuring the  $[O\ III]\ \lambda 4363/(\lambda 4959 + \lambda 5007)$  ratio. We have measured the temperature sensitive  $[O\ III]\ \lambda 4363$  line in HII regions in four of the five galaxies (6 of the 10 observed HII regions). For deriving the temperature in the  $[O\ III]$  zone, and all subsequent

abundance calculations, we use the emissivities determined from the five-level atom program of Shaw & Dufour (1995). The error in  $T_e(O^{++})$  is derived from the emission line uncertainties and does not include terms for uncertainties in the atomic data nor for the presence of temperature variations within the [O III] zone. Following SK93, we use the formula derived by Pagel et al. (1992) for estimating the temperature in the low ionization zone based on the models of Stasińska (1990):

$$T_e(O^+) = 2(T_e^{-1}(O^{++}) + 0.8)^{-1} \quad (1)$$

where  $T_e$  is the electron temperature in units of  $10^4$  K. We also assume  $T_e(N^+)$  and  $T_e(S^+)$  are equal to  $T_e(O^+)$  (cf. Garnett 1992). In some cases, the error in  $T_e(O^+)$  is unrealistically small if calculated directly from the error in  $T_e(O^{++})$ , and a lower limit of 500 K in the error of  $T_e(O^+)$  is assumed. From the [S II] lines we can calculate electron densities which are generally in the low density regime, (less than  $150 \text{ cm}^{-3}$ ,  $1\sigma$ ). Ionic abundances for  $O^{++}$  and  $O^+$  were then computed from the emission line ratios and we derived the oxygen abundance  $\equiv O/H = O^{++}/H^+ + O^+/H^+$  for all regions with  $\lambda 4363$  observed. A summary of ionic and total abundances via the direct method is shown in Table 2.

In the absence of a direct measurement of the electron temperature, photoionization models can act as a guide to determining oxygen abundances (cf. Edmunds & Pagel 1984). This is discussed specifically in the case of low abundance H II regions by Skillman (1989) where it was demonstrated that, due to a low sensitivity to the hardness of the radiation field, the [O II] and [O III] line strengths can be combined to uniquely determine the ionization parameter and an “empirical” oxygen abundance. McGaugh (1991) has produced a grid of photoionization models and recommended using the ratios of  $([O \text{ III}] + [O \text{ II}])/H\beta \equiv (\lambda 4959 + \lambda 5007 + \lambda 3727)/H\beta \equiv R_{23}$  and  $[O \text{ III}]/[O \text{ II}] \equiv (\lambda 4959 + \lambda 5007)/\lambda 3727$  (hereafter O32) to estimate the oxygen abundance. Figure 3 shows this diagnostic diagram with the models of McGaugh (1991) plotted and the observations of all ten observed Sculptor Group dI HII regions plotted. We have used the McGaugh models to determine empirical oxygen abundances and associated statistical errors, and have listed them in Table 3.

Pilyugin (2000) has proposed a new calibration of the empirical oxygen abundance scale. After rearranging terms, Pilyugin’s calibration is:

$$12 + \log(O/H) = 6.35 + 3.19 \log\left(\frac{I(\lambda 4959 + \lambda 5007 + \lambda 3727)}{I(H\beta)}\right) - 1.74 \log\left(\frac{I(\lambda 4959 + \lambda 5007)}{I(H\beta)}\right) \quad (2)$$

We have added the oxygen abundances calculated via Pilyugin’s calibration to Table 3, and compared Pilyugin’s calibration to that of McGaugh in Figure 4. There are two significant and systematic differences between these two empirical calibrations for low metallicity HII regions. First, note that Pilyugin’s calibration extends to larger values of  $\log(R_{23})$ . This solves the well known problem that McGaugh’s grid does not cover the highest values of  $\log(R_{23})$  that are observed. Because Pilyugin’s calibration is entirely empirical, it covers the full range of the observations. The second significant difference is the change in slopes of the calibrations at low values of  $\log(O32)$ .

Since most of the calibrating observations used by Pilyugin had high values of  $\log(O32)$ , the extrapolation of his calibration into the lower  $\log(O32)$  regime is subject to very large uncertainty. Note, for example, the 0.34 dex difference between M91 and P00 for the low excitation HII regions NGC 625 #21. Because McGaugh's calibration is guided by photoionization models in this regime, it is probably the more accurate there.

Figure 5 shows the differences between the three oxygen determinations given in Table 3 as a function of both  $\log(O32)$  and  $\log(R_{23})$ . When the differences are plotted as a function of  $\log(O32)$ , the systematic difference between the M91 and P00 calibrations is obvious. As could also be seen in Figure 4, in some cases, the empirical oxygen abundances are in good agreement with the direct oxygen abundances, with a slight bias towards lower oxygen abundances from the direct measurements (i.e., the differences for ESO 471-G06 #2, ESO 473-G24 #2, and NGC 625 #18 all fall between -0.03 and -0.15 dex). The small bias could be indicative of any of a number of different effects. One possibility is the breakdown of the assumption of a uniform electron temperature (see Peimbert, Peimbert, & Luridiana 2002 and references therein). A second related possibility is the presence of a second heating source in addition to photoionization (Stasińska, Schaerer, & Leitherer 2001). A third possibility is that radiation fields are much softer than those considered by the models (McGaugh 1991 shows that this is a relatively small effect - compare the two models plotted in Figure 3 - but Stasińska et al. 2001 caution that use of only zero-age stellar models does not probe a large enough range in input stellar models).

However, there are some truly discrepant results which do require attention. ESO 347-G17 #5 shows a difference of -0.35 dex for the M91 calibration and -0.32 for the P00 calibration. On the other hand, the empirical abundances for HII region ESO 347-G17 #10 differ by 0.31 dex. The brightest two HII regions for NGC 625 also show significant discrepancies. The empirical abundances for NGC 625 #5 and #9 are between -0.19 to -0.35 dex below those of the direct oxygen abundances. It is interesting that the empirical oxygen abundances for the three brightest NGC 625 HII regions all agree within a range of 0.24 dex, while the direct oxygen abundances cover a range of 0.23 dex, but the order in oxygen abundance is different for each method.

These significant differences lead us to two important conclusions: First, we feel that both of the existing empirical oxygen abundance calibrations for metal poor HII regions have deficiencies and that the problem of calibrating the empirical oxygen abundances should be revisited with a much larger database consisting of observations spanning a large range in both  $\log(R_{23})$  and  $\log(O32)$ . Second, the uncertainties quoted when using empirical oxygen abundances probably have been underestimated in the past. McGaugh (1991) estimated an uncertainty of 0.05 dex for low metallicity HII regions. However, this was based on a comparison with the abundances of Campbell (1988). Although the observations used by Campbell did include measurements of the  $[O\ III]\ \lambda 4363$  line, Campbell's abundances were based on photoionization model fits to only the bright  $[O\ II]$  and  $[O\ III]$  lines. Thus, this estimate of the uncertainty is specious, and only shows the range in results of different photoionization model fits to the bright lines. Pilyugin (2000) claims that his calibration is as accurate as using the direct method, and this could be true for the regime of high values of

$\log(O32)$ , but this is almost certainly not true for lower values of  $\log(O32)$ .

All of the above are important to the question of whether abundances in dI galaxies are uniform or if there are real variations. Generally, dwarf irregular galaxies are observed to have uniform abundances (Kobulnicky & Skillman 1996, 1997; and references therein). However, given that usually only a handful of HII regions are observable in a dI and that only a percentage of them have  $[O\ III]\ \lambda 4363$  bright enough to be well measured, it is then problematic to seriously test the level of abundance variations. For example, are there abundance variations in NGC 625? Both the direct methods and the empirical methods would indicate that there are, but none of the methods are in agreement. Because the direct method is subject to several systematic uncertainties ( $\lambda 4363$  is an inherently weak line and, at low velocities, is liable to possible contamination by terrestrial Hg emission; the assumption of a single temperature in the  $O^{++}$  zone is probably not correct; the assumption of a single relationship between the temperature in the  $O^{++}$  and  $O^+$  zones is certainly only a first order assumption), a measurement of  $\lambda 4363$  should not be taken as *prima facie* evidence of an accurate oxygen abundance.

Nonetheless, given the present observations, is it possible that there are measurable differences in the oxygen abundances in NGC 625? Looking at the direct measurements, the two brightest HII regions (#5 and #9) are in excellent agreement, but the third HII region (#18) shows an electron temperature which is about 2,000 K higher, and thus an oxygen abundance about 0.2 dex lower. Is this result to be taken at face value? While the  $\lambda 4363$  line is relatively weak, there is no contaminating Hg emission, and the associated errors result in only a 0.04 dex error in the oxygen abundance. Is it possible that the brightest two HII regions have experienced some self-pollution? There is evidence from the spectra that the ionizing clusters in the two brightest HII regions are old enough that the most massive stars have evolved off the main sequence phase. Figure 6, a close-up in the region of  $\sim\lambda 4700$  in region #5, shows the presence of broad He II emission usually associated with the winds of massive early-type stars with ages of at least 2 million years. The equivalent width of the  $\lambda 4686$  feature is  $5.5 \pm 1.5$  Å, and there appears to be no evidence in the spectrum for the Wolf-Rayet emission features at  $\lambda 4640$  (N III),  $\lambda 4650$  (C III/C IV), or  $\lambda 5808$  (C IV) at the 0.1 Å level. Broad He II  $\lambda 4686$  emission is also detected in region #9, although at a much lower level (0.7 Å EW).

The lack of the W-R features associated with C and N is indicative of low metallicity (Maeder, Lequeux, & Azzopardi 1980; Arnault, Kunth, & Schild 1989), and, in the detailed models, these features tend to disappear at metallicities of around one-tenth of the solar value (Krüger, et al. 1992; Schaerer & Vacca 1998). Although it is undeniably desperate to attempt to infer abundances from the presence or absence of W-R features, the absence of these W-R features may favor the lower abundances (for the stars), implying that the nebular abundances could have been enhanced by the return of newly produced oxygen. However, the similar N/O abundances seen in the brightest 3 HII regions would argue against the recent enhancement (see next section).

Additionally, the empirical abundances give the opposite result in that the two brightest HII

regions are lower in oxygen abundance than the two fainter HII regions. Basically, in this case, it appears to be difficult to pin down the abundances at better than the 0.2 dex level, which is approximately the range of the measurements. Given the interest in the problem of “self-pollution” and its role in the chemical evolution of dwarf galaxies (e.g., Kunth & Sargent 1986, Tenorio-Tagle 1996, Recchi, Matteucci, & D’Ercole, 2001) a clearer view of the observational situation is probably warranted.

### 3.2. The N/O Abundance Ratio

#### 3.2.1. Theories of the N/O Ratios in Dwarf Galaxies

A rather substantial review of the observational and theoretical aspects of the N/O abundance ratio is given in Henry, Edmunds, & Köppen (2000). Here we list just a few important highlights. While the production of O in galaxies is dominated by nucleosynthesis in massive stars and relatively prompt return to the ISM via supernovae type II explosions, the dominant processes leading to the enrichment of N in galaxies is still debated. In the more massive spiral galaxies, at higher metallicities, N/O increases roughly linearly with O/H, indicative of a secondary production mechanism dominating N production (Vila-Costas & Edmunds 1993). This secondary production of N is expected to come from C and O in the CNO cycle in intermediate mass stars, with subsequent release into the ISM via red giant winds and planetary nebula. In contrast, dwarf irregular galaxies also show relatively constant N/O at low metallicities with increasing upward scatter at higher metallicities (Garnett 1990, Thuan et al. 1995, Kobulnicky & Skillman 1996). A constant value of N/O over a large range in metallicity could be taken as evidence of primary production of N (Pagel 1985).

Three processes leading to primary N production have been suggested. Renzini & Voli (1981) showed that increasing the convective scale length over the pressure scale length resulted in freshly synthesized  $^{12}\text{C}$  being brought up to the convective envelope whereupon it can be converted to N via the CNO cycle. This “hot bottom burning” mechanism (Iben & Renzini 1983) will be most effective in the mass range of 4 to 5 solar masses. Timmes, Woosley, & Weaver (1995) and Woosley & Weaver (1995) have suggested that primary N might be produced in massive stars (heavier than 30 solar masses) of low metallicity. Again, if convection is enlarged beyond the standard models, a convective, helium burning shell penetrates into the hydrogen burning shell, and freshly synthesized C is converted into N. Recently, Meynet & Maeder (2002) have shown that when the effects of stellar rotation are included, stars of metallicities lower than about 1/5th of solar are capable of producing a large amount of primary N due to enhanced shear mixing. Their mechanism is important for stars with masses between 2 and  $7\text{ M}_\odot$ . Note that the first and third primary N production processes would have comparable delivery times of a few 100 million years, while the second process would be of order 10 million years.

Garnett (1990) discussed the possibility that the spread in the values of N/O at a given O/H

as measured in dwarf irregulars could be attributed to a delay between the delivery of O and N to the ISM (as proposed by Edmunds & Pagel 1978). If a dwarf galaxy experiences a dominant global burst of star formation, then the ISM O abundance will increase after roughly 10 million years, with a resulting decrease in N/O. (This assumes that the O is immediately incorporated into a visible component of the ISM, i.e., the warm phase, which is argued against by Kobulnicky & Skillman 1997.) Then, over a period of several hundred million years, the N/O abundance ratio will increase at constant O/H (given the absence of a subsequent burst of star formation in that time interval). Under these assumptions (dominant bursts of star formation separated by quiescent periods and delayed N delivery to the ISM) the N/O ratio becomes a clock, measuring the time since the last major burst of star formation. Low values of N/O imply a recent burst of star formation, while high values of N/O imply a long quiescent period. If it takes the O a few tens of millions of years to be incorporated into a visible component of the ISM, then the “clock” will still be effective, but if it takes a few 100 million years for this to take place, then bursts are unlikely to drive the N/O variations. Since the N/O variations are observed, and appear to be real, this suggests that the O mixing time scale is short compared to the N release timescale.

Henry et al. (2000) have presented models which produce a plateau in N/O at low values of O/H with a steep rise in values of N/O at higher values of O/H by assuming both primary and secondary production of N by intermediate mass stars. For the case of bursting galaxies, they note that as long as the period between the bursts is longer than about 250 million years, then the N from the intermediate mass stars will have sufficient time to be released and mixed, so that even these galaxies should lie close to the trend established by their slowly decreasing star formation rate models. In order to explain the scatter in N/O at higher values of O/H, they favor a scenario of fast enrichment of N by Wolf-Rayet stars or luminous blue variable stars.

Larsen, Sommer-Larsen, & Pagel (2001) have recently investigated the problem, and, based on simultaneous constraints from N, O, and He abundances and the relationship between metallicity and gas mass fraction, they conclude that the scatter in N/O at given O is best understood by a double-bursting mode of star formation. In this scenario, a burst of star formation triggers a second burst with a delay of roughly 30 million years.

Hopefully, observations of abundance ratios in several HII regions in dwarf galaxies that are close enough to construct recent star formation histories (like the present sample of Sculptor dIs) will allow us to distinguish between these different interpretations.

### 3.2.2. *Our Results and Implications*

For the present discussion, we will concentrate on the higher quality spectra (those with  $\lambda 4363$  detected). In order to convert the  $N^+/O^+$  ionic abundance ratio into a total abundance ratio (N/O), we need to account for any differences in ionic fractions. We adopt the standard assumption:  $N^+/O^+ \equiv N/O$  (Garnett 1990). The N/O ratios are given in Table 2.

Figure 7 presents a comparison of the N/O and O/H in the Sculptor Group dIs with the collection of dwarf irregular galaxies and H II galaxies assembled by Kobulnicky & Skillman (1996; see their Table 5 and Figure 15 for identification of individual points). Also added to the figure are the low surface brightness dwarfs of van Zee et al. (1997b) and the low metallicity BCDs of Izotov & Thuan (1999, hereafter IT99). For three of the four galaxies, the results, considering errors, are relatively close to the average value of  $\text{N/O} = -1.47$  determined for dwarf irregular galaxies by Garnett (1990). More recent studies have found similar averages. Thuan et al. (1995) found an average of  $\log(\text{N/O}) = -1.53 \pm 0.08$  for a sample of 14 blue compact galaxies (BCGs). van Zee et al. (1997b) found an average of  $\log(\text{N/O}) = -1.56 \pm 0.11$  for their sample of low surface brightness dwarfs. In the present sample, only NGC 625 deviates significantly, with higher N/O ratios in all three of the observed HII regions. Nonetheless, each of the Sculptor Group galaxies are interesting in their right, and we will discuss them individually.

ESO 473-G24 presents a particularly interesting case. IT99 have derived an average of  $\log(\text{N/O}) = -1.60 \pm 0.02$  for a sample of 6 BCGs with  $12 + \log(\text{O/H}) \leq 7.6$ . Based on this, IT99 propose a scenario in which all galaxies with  $12 + \log(\text{O/H}) \leq 7.6$  are undergoing their first ever burst of star formation and their elemental abundance ratios represent pure primary production. ESO 473-G24 does not follow this pattern. For this galaxy, the empirical oxygen abundances for both HII regions and the direct oxygen abundance for the brighter HII region are all at or below  $12 + \log(\text{O/H}) = 7.6$ . However,  $\log(\text{N/O})$  is measured to be  $-1.43 \pm 0.03$ . The present observations of ESO 473-G24 show that not all galaxies with  $12 + \log(\text{O/H}) \leq 7.6$  have identical N/O abundance ratios.

In this regard, ESO 473-G24 is similar to DDO 154. Kennicutt & Skillman (2001) find that DDO 154 ( $12 + \log(\text{O/H}) = 7.67 \pm 0.05$ ) is elevated in N/O ( $= -1.44 \pm 0.05$ ) relative to the extremely narrow plateau defined by the low metallicity BCDs of IT99. However, the  $3.2\sigma$  difference is not striking and would be even less so if not for the very small dispersion (0.02 dex) in N/O for the IT99 sample. Kennicutt & Skillman (2001) have pointed out that the observed narrow dispersion in the IT99 observations itself is very difficult to understand given the associated uncertainties in reddening corrections, the ionization correction factor, and the estimated temperature in the  $\text{O}^+$  zone.

It is already well known that the Local Group dwarf galaxy Leo A has an oxygen abundance of  $12 + \log(\text{O/H}) \approx 7.3$  (Skillman et al. 1989; van Zee, Skillman, & Haynes 2002), and yet shows the bulk of its stars were formed over the last few Gyr (Tolstoy et al. 1998). Recently, Dolphin et al. (2002) have shown evidence for an ancient (age  $\sim 10$  Gyr) stellar population in Leo A. This implies that the IT99 scenario is certainly not universal, and casts doubt on the conclusion that the N observed in low metallicity galaxies was all produced recently in massive stars.

The high N/O ratio seen in all three of the HII regions of NGC 625 is notable in that it lies close to the upper envelope of values observed in dIs and blue compact galaxies. Although the N/O ratio is not as high as the extreme of  $\log(\text{N/O}) = -0.85$  seen in one region of NGC 5253 (Kobulnicky et

al. 1997 and references therein), it does lie in a part of the diagram populated only by blue compact galaxies. There are alternative possible explanations for the high N/O in NGC 625. On one hand, it may be that a long quiescent period is required before a galaxy can experience such a strong burst of star formation like that seen in NGC 625. In this case, the N/O ratio would reach its maximum as the delayed nitrogen production has the opportunity to come to completion. The alternative is that something similar to the case of NGC 5253 has occurred, where prompt enrichment of N is observed (i.e., N released from the winds of the massive stars exciting the HII region is responsible for “polluting” the local gas to a higher value than the surrounding ISM). The similarity of the N/O ratios in the different HII regions of NGC 625 imply that the former possibility is more likely (in NGC 5253 the surrounding “normal” HII regions have  $\log (N/O) = -1.3$ ). An HST study of NGC 625 is now underway (Cannon et al. 2002), and it will be interesting to compare the estimates of the ages of the exciting cluster stars in each of the observed HII regions.

If the hypothesis of delayed N production holds up as the explanation for NGC 625, it would join other observational studies which point to N production predominantly in intermediate mass stars. Based on the observation of high N/O in the Pegasus dwarf irregular galaxy, Skillman et al. (1997) have proposed that dwarf galaxies with low current star formation rates may be a good location to look for enhanced N/O. From HST observations, Gallagher et al. (1998) found that the star formation rate in the Pegasus dwarf irregular galaxy has been relatively low for the last few 100 million years, supporting the hypothesis of high N/O due to delayed N production. Although ESO 473-G24 and ESO 471-G06 lack detailed studies of their stellar populations, they both have extremely low current star formation rates for their total gas content resulting in a gas depletion time scales of 65 Gyr and 110 Gyr, respectively (cf. paper 1, Table 3). Their N/O ratios appear to be at least consistent with the proposal that we are seeing the effects of completed delayed N production in these relatively low metallicity systems.

In this regard, the galaxies with relatively *low* values of N/O may hold the key to understanding the scatter in N/O. If a galaxy is observed a sufficient amount of time after a burst to allow the O to be released and mixed, but not too long such that N production hasn’t reached its peak, a low N/O is predicted by the delayed delivery hypothesis. Skillman, Terlevich, & Melnick (1989) suggested that this might be the case in NGC 6822, and Gallart et al. (1996) showed evidence for a significant increase in the star formation rate during the period 100 to 200 million years ago. With its low N/O ratio, ESO 347-G17 may present another target worthy of constructing a recent star formation history. Although it appears to lie at the back of the Sculptor Group, with a nominal distance of 7 Mpc (paper 1), it is close enough that a reliable recent star formation history can be constructed from Hubble Space Telescope observations (e.g., Dohm-Palmer et al. 1997, 1998).

If the evidence presented here favors the delayed N production as an explanation of the observed scatter in N/O, then does this compare with regard to Henry et al.’s observation that the data are better understood in terms of N contamination and not O contamination? They favor N contamination because the majority of excursions away from their trend line are upward (increasing N), not downward (increasing O). We have two observations to add here. First, in the regime of 7.5

$\leq 12 + \log (\text{O/H}) \leq 8.3$ , the situation is not so clear, with large numbers of excursions both above and below their model trend line. Second, the observations in this regime are heavily weighted toward blue compact galaxies. If typical burst durations are closer to 100 million years than to 10 million years (e.g., NGC 1569, Vallenari & Bomans, 1996; Greggio et al. 1998) then the observations may present a biased sample and the mean N/O in this range may be higher than the mean in the sample. Henry et al. (2000) preface their conclusion with the caveat that their interpretation assumes no selection effects in their compilation of observations.

### 3.3. Other Relative Abundances

The  $\log (\text{S/O})$  abundance ratios in Table 2 vary between  $-1.36$  and  $-1.55$ . This is comparable to the range of  $-1.45$  to  $-1.60$  observed in low metallicity BCDs by Thuan et al. (1995). These all support the observation of Garnett (1989) that the S/O ratio shows no dependence on metallicity and likely reflects the relative yields of S and O in massive stars.

Since the value of the helium abundance requires an accuracy of a few percent to be of use in constraining big bang nucleosynthesis, and since different methods of analysis produce variations of order a few percent (Peimbert, Peimbert, & Ruiz 2000; Olive & Skillman 2001), we have not calculated He abundances for these observations. Most of the HII regions are low surface brightness, and therefore will not provide a useful constraint on the primordial He abundance. The brightest region in NGC 625 is the exception, with very high s/n in even its faint HeI lines (e.g.,  $\lambda 4026, 7065$ ). We defer a detailed analysis of the helium abundance in NGC 625 to a later paper. Note that with an electron temperature of  $\sim 11,000\text{K}$ , the HII region in NGC 625 lies in the regime where temperature fluctuations will be very small (Peimbert, Peimbert, & Luridiana 2002). Thus, this object may be very useful in this regard.

## 4. The Metallicity – Luminosity Relationship for Dwarf Irregular Galaxies

Since the nebular abundance studies of the Magellanic Clouds in the mid 1970's (e.g., Peimbert & Torres-Peimbert 1974, 1976), it has been suggested that there might be a correlation between galaxian mass and the metallicity of the interstellar medium. This has been supported by observations of H II regions in irregular galaxies by Lequeux et al. (1979), Talent (1980), Kinman & Davidson (1981), Skillman et al. (1989), Richer & McCall (1995), Miller (1996), and van Zee et al. (1997b). There have been suggestions that the fundamental relationship may not be between mass and metallicity, but between surface density and metallicity (Mould, Kristian, & DaCosta 1983; Bothun & Mould 1988; Edmunds & Phillips 1989). Based on observations of two dEs in the M81 group, Caldwell et al. (1998) concluded that luminosity, and not surface brightness, is the key parameter determining metallicity for the dEs.

Kennicutt & Skillman (2001), drawing on observations from the literature, concluded that

luminosity, and not surface brightness, is probably the important parameter for determining metallicity in dIs also. In Figure 8, we compare our new observations of the Sculptor Group dIs to the compilation of Local Group dIs by Mateo (1998). We have added in the oxygen abundance for the Sculptor Group dI A143 = ESO 245-G05 (see paper 1) reported by Miller (1996) as  $12 + \log(\text{O/H}) = 7.97$ . Once again, while the known correlation in O/H versus L is clearly shown, the correlation is much weaker (or absent) for O/H versus surface brightness. It would appear that this comparative study supports luminosity as the important parameter.

It would be best to place this conclusion on a firmer statistical base, but the sample size is small and non-uniform. In order to investigate only the scatter in Figure 8, we have assumed errors of 0.1 dex in all of the abundance measurements and 0.2 mag in the luminosities and surface brightness. Then performing a linear least squares fit to both samples yields nearly identical values of  $\chi^2$  (60), even though the sample with luminosities is larger (19 versus 13). Running the same test on only the galaxies with both luminosities and surface brightnesses yields a factor of two lower  $\chi^2$  for the regression against luminosity (confirming what the eye sees in Figure 8). We repeat that it would be best to perform this type of test with a larger database with uniform error estimates.

## 5. The Chemical Evolution of Dwarf Irregular Galaxies

There has been a long standing debate concerning the role of galactic winds in the evolution of dwarf galaxies (see Skillman 1997 for a review). One aspect of this debate concerns the yields derived from the observations of dwarf galaxies. Often, the calculated yields are significantly lower than theoretically expected yields, and this has been taken as good evidence of losses due to metal enriched winds (Matteucci & Chiosi 1983).

In the simple closed box model with instantaneous recycling (Searle & Sargent 1972), the gas phase abundance ( $Z$ ) is related directly to the baryonic gas mass fraction ( $\mu$ ) as:

$$Z = y \ln\left(\frac{1}{\mu}\right) = y \ln\left(\frac{M_{\text{stars}}}{M_{\text{gas}}} + 1\right), \quad (3)$$

where  $y$  is the elemental yield. In principle, the heavy element yield can be derived from the present observations of the dI galaxies. This requires various assumptions, some of which are particularly tenuous (see, e.g., Kennicutt & Skillman 2001). For example, in order to derive the total gas mass, the HI mass is corrected for the presence of He (which is quite reasonable), and the fraction of gas mass in the molecular and hot phases is assumed to be small (probably less secure). It is also generally assumed that the entire HI disk has the metallicity as measured in the HII regions (which is quite uncertain, especially for very extended HI disks). And, finally, the conversion from optical luminosity to stellar mass carries a fair degree of uncertainty. If the assumptions of the simple closed box model are not appropriate, then the yield derived in this way is referred to as the “effective” yield.

In the study of DDO 154, Kennicutt & Skillman produced a simple diagnostic diagram of  $M(\text{HI})/L(\text{B})$  versus  $\log(\text{O}/\text{H})$  which, roughly, corresponds to gas mass fraction versus metallicity. There, it was shown that DDO 154 was consistent with a simple closed box model of chemical evolution with an effective yield ( $y = 4.2 \times 10^{-4}$ ) that was close to that predicted theoretically. van Zee et al. (1997a) showed this to be true for a number of LSB dIs and questioned the notion that these galaxies lose a large fraction of their gas mass due to galactic winds. In Figure 9, we present a similar graph comparing the Sculptor Group dIs with the Local Group dIs from the compilation of Mateo (1998)<sup>3</sup>, and the LSB dwarf irregulars from van Zee et al. (1997a). Superimposed on this comparison is the chemical evolution track for a simple closed box model derived for the very gas rich, low surface brightness dI DDO 154 (Kennicutt & Skillman 2001). For this model an effective oxygen yield of  $4.2 \times 10^{-4}$ , or roughly 50% of the solar value was used<sup>4</sup>. This is close to favored values for the theoretical or “true” yield (c.f. Maeder 1992), and was derived from estimates of the total stellar mass, the total gas mass, and the assumption of constant metallicity throughout the gas disk for DDO 154. An additional model with a factor of 3 lower yield ( $1.4 \times 10^{-4}$ ) has also been plotted in Figure 9. Most of the Sculptor Group dIs and LSB dIs lie between these two models.

There are two notable features to the distribution of Sculptor Group dIs in Figure 9. The first is the average displacement of the Sculptor Group dIs on the vertical axis relative to the Local Group dIs. The Sculptor Group dIs are very similar in gas content to the HI-rich low surface brightness galaxies studied by van Zee et al. (1997a,b). This is especially noteworthy since the van Zee et al. (1997a) sample was selected specifically from galaxies with the largest HI gas contents. While galaxies of this type appear to be common in the Sculptor Group, clearly it is rare to find Local Group dwarf galaxies with such large HI gas contents. Of the Local Group sample, only NGC 3109 has a comparably large HI gas content.

Second, of the Sculptor Group dIs observed so far, there appears to be a complete absence of the low metallicity, low gas content galaxies which are common in the Local Group (e.g., Leo A, Sag DIG, and the other galaxies in the lower left corner of Figure 9). Although we have not yet obtained spectra for all of the lowest luminosity (and therefore lowest metallicity) dIs in the Sculptor Group, we have not applied a bias for selecting against these galaxies. At this point, the relative lack of low metallicity, low gas content galaxies in the Sculptor Group appears to be real. Note that there are different ways in which to produce low metallicity, low gas content galaxies. Although a favored method is loss of metals, loss of HI gas can produce the same result. If the low gas contents of these galaxies are attributable to one of these other processes besides galactic winds (e.g., ram pressure stripping, Lin & Faber 1983, or “tidal stirring”, Mayer et al. 2001a,b)

---

<sup>4</sup>The value of  $M(\text{HI})/L(\text{B})$  for SagDIG in Table 4 of Mateo (1998) of 8.6 is in error, and we use the corrected value of 0.86 here.

<sup>4</sup>For the recently favored value of the solar abundance of  $4.9 \times 10^{-4}$  (Allende Prieto, Lambert, & Asplund 2001), this is equivalent to 86% of the solar value.

then this lack of low metallicity, low gas content dIs in the Sculptor Group could be a result of the lower density environment.

Although the Sculptor Group dIs and the LSB dIs lie close to the higher yield simple closed box model in Figure 9, the effective yields for many of them do leave some room for some deviation from the simple closed box model as either selective loss of metals or stripping of HI. Also note the following shortcoming of this simple diagram with regard to the assumption that  $M(\text{HI})/L(\text{B})$  gives a close approximation to gas mass fraction. In the case of NGC 625, low value of  $M(\text{HI})/L(\text{B})$  is due to its enhanced luminosity because of the recent burst of star formation, and it lies right next to the Pegasus dI with a low  $M(\text{HI})/L(\text{B})$  due to a truly low gas mass fraction. It is very likely that NGC 625, with an active starburst, has a much lower value of  $M/L$  than most of the other galaxies plotted in Figure 9. Thus it would be better represented by a higher yield model than its present position indicates. Replacing  $L(\text{B})$  with I band or K band luminosity would likely reduce the impact of the recent star formation on this diagnostic diagram. Surface photometry of these relatively low surface brightness systems at longer wavelengths, while difficult, is still highly desirable.

## 6. Conclusions

Using the CTIO 4-m, we have obtained optical spectroscopy of HII regions in five dI galaxies in the nearby Sculptor Group. From these spectra we derive oxygen, nitrogen, and sulfur abundances. Oxygen abundances are derived via three different methods (the “direct” method, the empirical method guided by photoionization modeling of McGaugh (1991), and the purely empirical method of Pilyugin (2000)) and are compared. Significant systematic differences are found between the three methods, and we suggest that a recalibration of the empirical abundance scale is required. Until differences between these three methods are better understood, the issue of the degree of uniformity of the ISM abundances in a dwarf galaxy cannot be properly addressed.

The N/O ratio in ESO 473-G24, which is a very metal poor galaxy, is found to be in the normal range for dwarf irregular galaxies, but elevated when compared to the very narrow range found by IT99 for low metallicity BCGs. This shows that not all galaxies with  $12 + \log(\text{O/H}) \leq 7.6$  have identical elemental abundance ratios, and this implies that the Izotov & Thuan scenario for low metallicity galaxies is not universal.

Measurements of the HII regions in NGC 625 yield  $\log(\text{N/O}) \approx -1.25$ . This relatively high N/O ratio may be indicative of a long quiescent period prior to the recent active burst of star formation. Altogether, the observations presented here and in the literature can be seen to support the scenario of N produced by intermediate mass stars. The large scatter in N/O at a given O/H is still consistent with contamination by O followed by later contamination by N. This is in agreement with what is observed in the high redshift damped Ly $\alpha$  systems (see Pettini et al. 2002 and references therein) and resolves the conflict between high and low redshift observations

discussed by Pilyugin (1999).

The oxygen abundances in the Sculptor Group dIs are in good agreement with the relationship between metallicity and luminosity observed in the Local Group dIs. Taken together the observations show a better relationship between metallicity and luminosity than between metallicity and galaxy central surface brightness.

The gas contents of the Sculptor Group dIs are large compared to the Local Group dIs. Many of the Sculptor Group dIs lie close to the evolutionary path predicted by a simple closed box model with an effective oxygen yield that is close to the theoretically favored values. It is possible that some of the Sculptor Group dwarfs are evolving nearly as closed systems. On the other hand, if the abundances in their extended HI disks are lower than in the HII regions, the appropriate value of the effective yield would be much smaller. The higher gas contents, lower average star formation rates, and closer resemblance to closed box evolution for Sculptor Group dIs relative to Local Group dIs could all be indicative of evolution in a relatively lower density environment.

We are grateful for the help of CTIO staff members Manuel Hernandez and Ricardo Venegas. We wish to thank G. Bothun, M. Edmunds, D. Garnett, R. Henry, R. Kennicutt, E. Tolstoy, and L. van Zee for many helpful conversations. John Cannon, Herny Lee, and Liese van Zee proofread and provided valuable comments on this manuscript. We also thank the referee for a prompt and careful reading of the manuscript and their valuable quibbles. This research has made use of the NASA/IPAC Extragalactic Database (NED) which is operated by the Jet Propulsion Laboratory, California Institute of Technology, under contract with the National Aeronautics and Space Administration. This research has made use of NASA's Astrophysics Data System Abstract Service. EDS acknowledges partial support from a NASA LTSARP grant No. NAG5-9221 and the University of Minnesota. BWM is supported by the Gemini Observatory, which is operated by the Association of Universities for Research in Astronomy, Inc., on behalf of the international Gemini partnership of Argentina, Australia, Brazil, Canada, Chile, the United Kingdom, and the United States of America.

## REFERENCES

Allende Prieto, C., Lambert, D. L., & Asplund, M. 2001, *ApJL*, 556, L63

Arnault, Ph., Kunth, D., & Schild, H., 1989, *A&A*, 224, 73

Bothun, G. D., & Mould, J. R. 1988, *ApJ*, 324, 123

Caldwell, N., Armandroff, T. E., Da Costa, G. S., & Seitzer, P. 1998, *AJ*, 115, 535

Campbell, A. 1988, *ApJ*, 335, 644

Cannon, J. M., Skillman, E. D., Dohm-Palmer, R. C., Côté, S., Miller, B. W., & Bomans, D. 2002, in prep.

Dekel, A., & Silk, J. 1986, *ApJ*, 303, 39

Dinerstein, H. L. 1990 in The Interstellar Medium in Galaxies, eds. H. A. Thronson, Jr., & J. M. Shull, Kluwer, 257

Dohm-Palmer, R. C. et al. 1997, *AJ*, 114, 2527

Dohm-Palmer, R. C. et al. 1998, *AJ*, 116, 1227

Dolphin, A. E., Saha, A., Claver, J., Skillman, E. D., Cole, A. A., Gallagher, J. S., Tolstoy, E., Dohm-Palmer, R. C., & Mateo, M. 2002, *AJ*, 123, 3154

Edmunds, M. G., & Pagel, B. E. J. 1978, *MNRAS*, 185, 78p

Edmunds, M. G., & Pagel, B. E. J. 1984, *MNRAS*, 211, 507

Edmunds, M. G., & Phillips, S. 1989, *MNRAS*, 241, 9p

Filippenko, A.V. 1982, *PASP*, 94, 715

Gallagher, J. S., Tolstoy, E., Dohm-Palmer, R. C., Skillman, E. D., Cole, A., Hoessel, J., Saha, A., & Mateo, M. 1998, *AJ*, 115, 1869

Gallart, C., Aparicio, A., Bertelli, G., & Chiosi, C. 1996, *AJ*, 112, 2596

Garnett, D. R. 1989, *ApJ*, 345, 282

Garnett, D. R. 1990, *ApJ*, 363, 142

Garnett, D. R. 1992, *AJ*, 103, 1330

González-Delgado, R. M., Leitherer, C., & Heckman, T. M. 1999, *ApJS*, 125, 489

Greggio, L., Tosi, M., Clampin, M., de Marchi, G., Leitherer, C., Nota, A., & Sirianni, M. 1998, *ApJ*, 504, 725

Henry, R. B. C., Edmunds, M. G., & Köppen, J. 2000, *ApJ*, 541, 660

Hidalgo-Gamez, A.M., & Olofsson, K. 1998, *A&A*, 334, 45

Howarth, I. D. 1983, *MNRAS*, 203, 301

Hummer, D. G. & Storey, P. J. 1987, *MNRAS*, 224, 801

Hunter, D. A., & Hoffman, L. 1999, AJ, 117, 2789

Iben, I. Jr., & Renzini, A. 1983, ARA&A, 21, 271

Izotov, Y. I., & Thuan T. X., 1999, ApJ, 511, 639 (IT99)

Kennicutt, R.C. Jr., & Skillman, E.D. 2001, AJ, 121, 1461

Kinman, T. D., & Davidson, K. 1981, AJ, 243, 127

Kobulnicky, H. A., & Skillman, E. D. 1996, ApJ, 471, 211

Kobulnicky, H. A., & Skillman, E. D. 1997, ApJ, 489, 636

Kobulnicky, H. A., & Skillman, E. D. 1998, ApJ, 497, 601

Kobulnicky, H. A., Skillman, E. D., Roy, J.-R., Walsh, J. R., & Rosa, M. R. 1997, ApJ, 477, 679

Krüger, H., Fritze-v. Alvensleben, U., Fricke, K. J., & Loose, H.-H. 1992, A&A, 259, L73

Kunth, D., & Sargent, W. L. W. 1986, ApJ, 300, 496

Larsen, T.I., Somer-Larsen, J., & Pagel, B.E.J. 2001, MNRAS, 323, 555

Larson, R. B. 1974, MNRAS, 169, 229

Lequeux, J. Peimbert, M., Rayo, J. F., Serrano, A., & Torres-Peimbert, S. 1979, A&A, 80, 155

Lin, D. N. C. & Faber, S. M. 1983, ApJ, 266, L21

Lu, L., Sargent, W. L. W., & Barlow, T. A. 1998, AJ, 115, 55

Maeder, A. 1992, A&A, 264, 105

Maeder, A., Lequeux, J., & Azzopardi, M. 1980, A&A, 90, 117

Mateo, M. 1998, ARA&A, 36, 435

Matteucci, F., & Chiosi, C. 1983, A&A, 123, 121

Mayer, L., Governato, F., Colpi, M., Moore, B., Quinn, T., Wadsley, J., Stadel, J., & Lake, G. 2001a, ApJ, 547, L123

Mayer, L., Governato, F., Colpi, M., Moore, B., Quinn, T., Wadsley, J., Stadel, J., & Lake, G. 2001b, ApJ, 559, 754

McGaugh, S. S. 1991, ApJ, 380, 140

Meynet, G., & Maeder, A. 2002, a&A, 381, L25

Miller, B. W. 1996, AJ, 112, 991

Mould, J. R., Kristian, J., and Da Costa, G. S. 1983, ApJ, 270, 471

Oke, J. B. 1990, AJ, 99, 1621

Olive, K. A., & Skillman, E. D. 2001, New Astronomy, 6, 119

Pagel, B. E. J. 1985 in, Production and Distribution of C, N, & O Elements, eds. I. J. Danziger, F. Matteucci, & K. Kjär, ESO, 155

Pagel, B. E. J., Simonson, E. A., Terlevich, R. J., & Edmunds, M. G. 1992, MNRAS, 255, 325

Peimbert, M., Peimbert, A., & Ruiz, M. 2000, ApJ, 541, 688

Peimbert, M., Peimbert, A., & Luridiana, V. 2002, ApJ, 565, 668

Peimbert, M., & Torres-Peimbert, S. 1974, ApJ, 193, 327

Peimbert, M., & Torres-Peimbert, S. 1976, ApJ, 203, 581

Pettini, M., Lipman, K., & Hunstead, R. W. 1995, ApJ, 451, 100

Pettini, M., Rix, S., Steidel, C. C., Adelberger, K. L., Hunt, M. P., & Shapley, A. E. 2002, ApJ, 569, 742

Pilyugin, L.S. 1999, A&A, 346, 428

Pilyugin, L.S. 2000, A&A, 362, 325

Pilyugin, L.S. 2001, A&A, 374, 412

Recchi, S., Matteucci, F., & D’Ercole, A. 2001, MNRAS, 322, 800

Renzini, A., & Voli, M. 1981, A&A, 94, 175

Richer, M. G., & McCall, M. L. 1995, ApJ, 445, 642

Schaerer, D., & Vacca, W. D. 1998, ApJ, 497, 618

Schlegel, D.J., Finkbeiner, D.P., & Davis, M. 1998, ApJ, 500, 525

Seaton, M. J. 1979, MNRAS, 187, 73p

Searle, L., & Sargent, W. L. W. 1972, ApJ, 173, 25

Shaw, R. A., & Dufour, R. J. 1995, PASP, 107, 896

Skillman, E. D. 1989, ApJ, 347, 883

Skillman, E. D. 1997, RevMexAASC, 6, 36

Skillman, E. D. 1998, in, Stellar Astrophysics for the Local Group, eds. A. Aparicio, A. Herrero, & F. Sánchez, Cambridge University Press, 457

Skillman, E. D., Bomans, D. J., & Kobulnicky, H. A. 1997, ApJ, 474, 205

Skillman, E. D., Côté, S., & Miller, B.W. 2002, AJ, submitted (paper 1)

Skillman, E. D., & Kennicutt, R. C. 1993, ApJ, 411, 655 (SK93)

Skillman, E. D., Kennicutt, R. C., & Hodge, P. W. 1989a, ApJ, 347, 875

Skillman, E. D., Kennicutt, R. C. Jr., Shields, G. A., & Zaritsky, D. 1996, ApJ, 462, 147

Skillman, E. D., Terlevich, R. J., & Melnick, J. 1989b, MNRAS, 240, 563

Stasińska, G. 1990, A&AS, 83, 501

Stasińska, G., Schaerer, D., & Leitherer, C. 2001, A&A, 370, 1

Talent, D. L. 1980, Ph.D. Thesis, Rice University

Tenorio-Tagle, G. 1996, AJ, 111, 1641

Thuan T. X., Izotov, Y. I., & Lipovetsky 1995, ApJ, 445, 108

Timmes, F. X., Woosley, S. E., & Weaver, T. A. 1995, ApJS, 98, 617

Tolstoy, E., Gallagher, J. S., Cole, A. A., Hoessel, J. G., Saha, A., Skillman, E. D., Dohm-Palmer, R. C., & Mateo, M., & Hurley-Keller, D. 1998, AJ, 116, 1244

Vallenari, A. & Bomans, D. J. 1996, A&A, 313, 713

van Zee, L., Haynes, M. P., & Salzer, J. J. 1997a, AJ, 114, 2479

van Zee, L., Haynes, M. P., & Salzer, J. J. 1997b, AJ, 114, 2497

van Zee, L., Skillman, E.D., & Haynes, M. P. 2002, in prep

Vila-Costas, M. B., & Edmunds, M. G. 1993, MNRAS, 265, 199

Vilchez, J. M. 1995, AJ, 110, 1090

Woosley, S. E., & Weaver, T. A. 1995, ApJS, 101, 181

Table 1a. Corrected Relative Emission Line Fluxes and Errors

Wavelength	$f(\lambda)$	ESO 347-G17 #5 $I(\lambda)/I(H\beta)$	ESO 347-G17 #10 $I(\lambda)/I(H\beta)$	ESO 348-G09 #3 $I(\lambda)/I(H\beta)$
3727 [O II]	0.267	$4.204 \pm 0.131$	$3.079 \pm 0.151$	$2.941 \pm 0.159$
3868 [Ne III]	0.240	$0.404 \pm 0.019$	$0.359 \pm 0.034$	...
3889 H8 + He I	0.237	$0.271 \pm 0.015$	$0.332 \pm 0.030$	...
3969 [Ne III] + H7	0.221	$0.269 \pm 0.013$	...	...
4101 H $\delta$	0.193	$0.242 \pm 0.012$	$0.258 \pm 0.023$	$0.262 \pm 0.027$
4340 H $\gamma$	0.137	$0.488 \pm 0.015$	$0.463 \pm 0.023$	$0.459 \pm 0.027$
4363 [O III]	0.137	$0.061 \pm 0.006$	...	...
4471 He I	0.109	$0.030 \pm 0.005$	...	...
4861 H $\beta$	0.000	$1.000 \pm 0.022$	$1.000 \pm 0.026$	$1.000 \pm 0.029$
4959 [O III]	-0.022	$1.018 \pm 0.022$	$1.587 \pm 0.037$	$0.428 \pm 0.017$
5007 [O III]	-0.022	$3.086 \pm 0.063$	$3.790 \pm 0.081$	$1.093 \pm 0.030$
5876 He I	-0.225	$0.064 \pm 0.003$	$0.073 \pm 0.007$	...
6300 [O I]	-0.292	$0.046 \pm 0.003$	...	...
6312 [S III]	-0.292	$0.019 \pm 0.002$	...	...
6363 [O I]	-0.301	$0.016 \pm 0.002$	...	...
6548 [N II]	-0.329	$0.035 \pm 0.003$	$0.029 \pm 0.005$	...
6563 H $\alpha$	-0.329	$2.796 \pm 0.091$	$2.809 \pm 0.141$	$2.809 \pm 0.148$
6584 [N II]	-0.329	$0.116 \pm 0.005$	$0.103 \pm 0.008$	$0.173 \pm 0.012$
6678 He I	-0.346	$0.026 \pm 0.002$	...	...
6717 [S II]	-0.351	$0.355 \pm 0.013$	$0.207 \pm 0.013$	$0.295 \pm 0.019$
6731 [S II]	-0.351	$0.243 \pm 0.009$	$0.205 \pm 0.013$	$0.186 \pm 0.013$
7065 He I	-0.396	$0.022 \pm 0.002$	...	...
$F(H\beta)$ (erg cm $^{-2}$ s $^{-1}$ )	...	$3.4 \times 10^{-15}$	$1.0 \times 10^{-15}$	$4.2 \times 10^{-16}$
$C(H\beta)$	...	$0.29 \pm 0.03$	$0.26 \pm 0.06$	$0.16 \pm 0.06$
$EW(H\beta)$ (Å)	...	$30 \pm 1$	$15 \pm 1$	$26 \pm 1$
$EW(H \text{ abs})$ (Å)	...	$0.3 \pm 0.3$	$0.8 \pm 0.4$	$1.5 \pm 0.6$

Table 1b. Corrected Relative Emission Line Fluxes and Errors

Wavelength	$f(\lambda)$	ESO 471-G06 #2 $I(\lambda)/I(H\beta)$	ESO 473-G24 #2 $I(\lambda)/I(H\beta)$	ESO 473-G24 #4 $I(\lambda)/I(H\beta)$
3727 [O II]	0.267	$2.072 \pm 0.075$	$1.109 \pm 0.044$	$1.138 \pm 0.072$
3798 H10	0.253	...	...	...
3835 H9	0.248	$0.072 \pm 0.006$	$0.061 \pm 0.006$	...
3868 [Ne III]	0.240	$0.225 \pm 0.010$	$0.210 \pm 0.011$	$0.184 \pm 0.023$
3889 H8 + He I	0.237	$0.190 \pm 0.008$	$0.202 \pm 0.010$	$0.277 \pm 0.026$
3969 [Ne III] + H7	0.221	$0.189 \pm 0.008$	$0.201 \pm 0.009$	$0.147 \pm 0.019$
4101 H $\delta$	0.193	$0.253 \pm 0.009$	$0.268 \pm 0.010$	$0.272 \pm 0.021$
4340 H $\gamma$	0.137	$0.469 \pm 0.013$	$0.471 \pm 0.014$	$0.441 \pm 0.021$
4363 [O III]	0.137	$0.050 \pm 0.003$	$0.058 \pm 0.004$	...
4471 He I	0.109	$0.032 \pm 0.003$	$0.036 \pm 0.003$	$0.050 \pm 0.011$
4861 H $\beta$	0.000	$1.000 \pm 0.021$	$1.000 \pm 0.021$	$1.000 \pm 0.026$
4959 [O III]	-0.022	$0.848 \pm 0.018$	$0.769 \pm 0.016$	$0.566 \pm 0.017$
5007 [O III]	-0.022	$2.654 \pm 0.054$	$2.291 \pm 0.047$	$1.838 \pm 0.043$
5876 He I	-0.225	$0.096 \pm 0.003$	$0.093 \pm 0.003$	$0.082 \pm 0.007$
6300 [O I]	-0.292	$0.025 \pm 0.001$	$0.010 \pm 0.001$	...
6312 [S III]	-0.292	$0.015 \pm 0.001$	$0.012 \pm 0.001$	$0.025 \pm 0.005$
6363 [O I]	-0.301	$0.010 \pm 0.001$	...	...
6548 [N II]	-0.329	$0.032 \pm 0.002$	$0.019 \pm 0.001$	...
6563 H $\alpha$	-0.329	$2.796 \pm 0.113$	$2.741 \pm 0.113$	$2.771 \pm 0.145$
6584 [N II]	-0.329	$0.098 \pm 0.004$	$0.046 \pm 0.002$	$0.032 \pm 0.005$
6678 He I	-0.346	$0.026 \pm 0.001$	$0.028 \pm 0.002$	...
6717 [S II]	-0.351	$0.181 \pm 0.008$	$0.070 \pm 0.003$	$0.095 \pm 0.007$
6731 [S II]	-0.351	$0.126 \pm 0.006$	$0.055 \pm 0.003$	$0.050 \pm 0.005$
7065 He I	-0.396	$0.018 \pm 0.001$	$0.028 \pm 0.002$	$0.016 \pm 0.004$
$F(H\beta)$ (erg cm $^{-2}$ s $^{-1}$ )	...	$5.7 \times 10^{-15}$	$2.3 \times 10^{-15}$	$4.2 \times 10^{-16}$
$C(H\beta)$	...	$0.11 \pm 0.05$	$0.19 \pm 0.05$	$0.14 \pm 0.06$
EW(H $\beta$ ) (Å)	...	$74 \pm 3$	$133 \pm 6$	$54 \pm 3$
EW(H abs) (Å)	...	$1.3 \pm 1.0$	$0.0 \pm 1.6$	$2.5 \pm 1.3$

Table 1c. Corrected Relative Emission Line Fluxes and Errors

Wavelength	f( $\lambda$ )	NGC 625 #5 I( $\lambda$ )/I(H $\beta$ )	NGC 625 #9 I( $\lambda$ )/I(H $\beta$ )	NGC 625 #18 I( $\lambda$ )/I(H $\beta$ )	NGC 625 #21 I( $\lambda$ )/I(H $\beta$ )
3727 [O II]	0.267	1.7574 $\pm$ 0.0585	2.3144 $\pm$ 0.0814	3.379 $\pm$ 0.121	4.861 $\pm$ 0.476
3750 H12	0.264	0.0300 $\pm$ 0.0013	0.0155 $\pm$ 0.0022	...	...
3771 H11	0.259	0.0346 $\pm$ 0.0014	0.0305 $\pm$ 0.0024	...	...
3798 H10	0.253	0.0489 $\pm$ 0.0018	0.0399 $\pm$ 0.0026	...	...
3820 He I	0.250	0.0116 $\pm$ 0.0007	...	...	...
3835 H9	0.248	0.0778 $\pm$ 0.0026	0.0663 $\pm$ 0.0031	0.067 $\pm$ 0.005	...
3868 [Ne III]	0.240	0.3268 $\pm$ 0.0103	0.1996 $\pm$ 0.0071	0.179 $\pm$ 0.008	...
3889 H8 + He I	0.237	0.1942 $\pm$ 0.0061	0.1841 $\pm$ 0.0065	0.185 $\pm$ 0.008	...
3969 [Ne III] + H7	0.221	0.2653 $\pm$ 0.0080	0.1953 $\pm$ 0.0066	0.172 $\pm$ 0.007	...
4026 HeI	0.208	0.0205 $\pm$ 0.0008	0.0161 $\pm$ 0.0017	...	...
4068 [S II]	0.200	0.0141 $\pm$ 0.0006	0.0165 $\pm$ 0.0016	0.029 $\pm$ 0.004	...
4101 H $\delta$	0.193	0.2581 $\pm$ 0.0072	0.2619 $\pm$ 0.0079	0.255 $\pm$ 0.009	0.295 $\pm$ 0.041
4340 H $\gamma$	0.137	0.4848 $\pm$ 0.0118	0.4718 $\pm$ 0.0120	0.469 $\pm$ 0.013	0.447 $\pm$ 0.038
4363 [O III]	0.137	0.0382 $\pm$ 0.0010	0.0219 $\pm$ 0.0013	0.034 $\pm$ 0.003	...
4387 He I	0.128	0.0050 $\pm$ 0.0003	...	...	...
4471 He I	0.109	0.0457 $\pm$ 0.0011	0.0395 $\pm$ 0.0015	0.040 $\pm$ 0.003	...
4658 [Fe III]	0.063	0.0048 $\pm$ 0.0003	0.0086 $\pm$ 0.0009	...	...
4713 [Ar IV] + He I	0.050	0.0073 $\pm$ 0.0003	0.0057 $\pm$ 0.0009	...	...
4861 H $\beta$	0.000	1.0000 $\pm$ 0.0200	1.0000 $\pm$ 0.0202	1.000 $\pm$ 0.020	1.000 $\pm$ 0.031
4921 He I	-0.001	0.0116 $\pm$ 0.0003	0.0079 $\pm$ 0.0008	...	...
4959 [O III]	-0.022	1.5225 $\pm$ 0.0305	0.9890 $\pm$ 0.0200	0.866 $\pm$ 0.018	0.331 $\pm$ 0.022
5007 [O III]	-0.022	4.5297 $\pm$ 0.0912	2.9520 $\pm$ 0.0596	2.547 $\pm$ 0.052	1.028 $\pm$ 0.032
5199 [N I]	-0.068	0.0052 $\pm$ 0.0002	0.0075 $\pm$ 0.0007	0.012 $\pm$ 0.001	...
5271 [Fe III]	-0.085	0.0017 $\pm$ 0.0002	...	...	...
5518 [Cl III]	-0.166	0.0041 $\pm$ 0.0002	0.0041 $\pm$ 0.0006	...	...
5538 [Cl III]	-0.169	0.0024 $\pm$ 0.0002	0.0027 $\pm$ 0.0006	...	...
5876 He I	-0.225	0.1164 $\pm$ 0.0035	0.1157 $\pm$ 0.0037	0.105 $\pm$ 0.004	0.084 $\pm$ 0.014
6300 [O I]	-0.292	0.0201 $\pm$ 0.0007	0.0168 $\pm$ 0.0008	0.046 $\pm$ 0.002	...
6312 [S III]	-0.292	0.0215 $\pm$ 0.0008	0.0201 $\pm$ 0.0009	0.017 $\pm$ 0.001	...
6363 [O I]	-0.301	0.0064 $\pm$ 0.0003	0.0047 $\pm$ 0.0005	0.011 $\pm$ 0.001	...
6548 [N II]	-0.329	0.0464 $\pm$ 0.0018	0.0706 $\pm$ 0.0029	0.084 $\pm$ 0.004	0.152 $\pm$ 0.021
6563 H $\alpha$	-0.329	2.8596 $\pm$ 0.1094	2.8447 $\pm$ 0.1152	2.818 $\pm$ 0.116	2.858 $\pm$ 0.333
6584 [N II]	-0.329	0.1235 $\pm$ 0.0047	0.2039 $\pm$ 0.0083	0.262 $\pm$ 0.011	0.422 $\pm$ 0.050
6678 He I	-0.346	0.0356 $\pm$ 0.0014	0.0337 $\pm$ 0.0015	0.029 $\pm$ 0.002	...
6717 [S II]	-0.351	0.1356 $\pm$ 0.0055	0.1966 $\pm$ 0.0084	0.341 $\pm$ 0.015	0.676 $\pm$ 0.085
6731 [S II]	-0.351	0.1010 $\pm$ 0.0041	0.1464 $\pm$ 0.0063	0.240 $\pm$ 0.011	0.521 $\pm$ 0.066
7065 He I	-0.396	0.0272 $\pm$ 0.0012	0.0262 $\pm$ 0.0014	0.017 $\pm$ 0.001	...
F(H $\beta$ ) (erg cm $^{-2}$ s $^{-1}$ )	...	$9.2 \times 10^{-14}$	$2.0 \times 10^{-14}$	$8.7 \times 10^{-15}$	$4.7 \times 10^{-16}$
C(H $\beta$ )	...	0.15 $\pm$ 0.04	0.01 $\pm$ 0.05	0.26 $\pm$ 0.05	0.32 $\pm$ 0.15
EW(H $\beta$ ) (Å)	...	235 $\pm$ 9	79 $\pm$ 3	37 $\pm$ 2	4.3 $\pm$ 0.3

Table 1c—Continued

Wavelength	$f(\lambda)$	NGC 625 #5 $I(\lambda)/I(H\beta)$	NGC 625 #9 $I(\lambda)/I(H\beta)$	NGC 625 #18 $I(\lambda)/I(H\beta)$	NGC 625 #21 $I(\lambda)/I(H\beta)$
EW(H abs) (Å)	...	0.0 ± 2.4	0.5 ± 0.3	0.8 ± 0.5	0.8 ± 0.5

Table 2. Ionic and Total Abundances

Property	ESO 347-G17 #5	ESO 471-G06 #2	ESO 473-G24 #2	NGC 625 #5	NGC 625 #9	NGC 625 #18
T(O III) (K)	15,170 $^{+840}_{-680}$	14,930 $^{+450}_{-400}$	17,080 $^{+620}_{-540}$	10,900 $^{+115}_{-109}$	10,460 $^{+213}_{-193}$	12,810 $^{+460}_{-395}$
T(O II) (K) (estimated)	13,370 $\pm$ 690	13,610 $\pm$ 500	14,440 $\pm$ 500	11,640 $\pm$ 500	11,390 $\pm$ 500	12,650 $\pm$ 500
T(S III) (K) (estimated)	14,300 $\pm$ 720	14,090 $\pm$ 500	15,880 $\pm$ 540	10,740 $\pm$ 500	10,380 $\pm$ 500	12,330 $\pm$ 500
n(S II)	$\leq$ 31 (1 $\sigma$ )	$\leq$ 61 (1 $\sigma$ )	156 $^{+102}_{-86}$	75 $^{+85}_{-72}$	75 $^{+90}_{-75}$	$\leq$ 84 (1 $\sigma$ )
O $^+$ /H $^+$ (x 10 $^5$ )	4.75 $\pm$ 0.77	2.40 $\pm$ 0.30	1.06 $\pm$ 0.12	3.52 $\pm$ 0.57	5.05 $\pm$ 0.85	5.00 $\pm$ 0.70
O $^{++}$ /H $^+$ (x 10 $^5$ )	3.18 $\pm$ 0.37	2.82 $\pm$ 0.19	1.79 $\pm$ 0.13	11.9 $\pm$ 0.44	8.89 $\pm$ 0.57	4.12 $\pm$ 0.37
O/H (x 10 $^5$ )	7.93 $\pm$ 0.86	5.22 $\pm$ 0.35	2.84 $\pm$ 0.18	15.4 $\pm$ 0.72	13.9 $\pm$ 1.03	9.12 $\pm$ 0.79
12 + log (O/H)	7.90 $\pm$ 0.09	7.72 $\pm$ 0.03	7.45 $\pm$ 0.03	8.19 $\pm$ 0.02	8.14 $\pm$ 0.03	7.96 $\pm$ 0.04
N $^+$ /O $^+$ (x 10 $^2$ )	2.28 $\pm$ 0.13	3.86 $\pm$ 0.22	3.68 $\pm$ 0.24	4.68 $\pm$ 0.27	5.68 $\pm$ 0.34	5.79 $\pm$ 0.34
log (N/O)	-1.64 $\pm$ 0.02	-1.41 $\pm$ 0.02	-1.43 $\pm$ 0.03	-1.33 $\pm$ 0.02	-1.25 $\pm$ 0.03	-1.24 $\pm$ 0.25
N/H (x 10 $^6$ )	1.81 $\pm$ 0.22	2.02 $\pm$ 0.18	1.05 $\pm$ 0.10	7.21 $\pm$ 0.53	7.92 $\pm$ 0.75	5.28 $\pm$ 0.55
S $^+$ /H $^+$ (x 10 $^7$ )	6.98 $\pm$ 0.77	3.64 $\pm$ 0.34	1.33 $\pm$ 0.13	3.83 $\pm$ 0.42	5.83 $\pm$ 0.67	7.91 $\pm$ 0.80
S $^{++}$ /H $^+$ (x 10 $^7$ )	12.50 $\pm$ 2.36	10.40 $\pm$ 1.38	5.85 $\pm$ 0.68	78.6 $\pm$ 7.31	41.8 $\pm$ 8.46	18.1 $\pm$ 2.86
ICF	1.15 $\pm$ 0.02	1.22 $\pm$ 0.02	1.27 $\pm$ 0.03	1.49 $\pm$ 0.05	1.28 $\pm$ 0.03	1.18 $\pm$ 0.02
S/H (x 10 $^6$ )	2.24 $\pm$ 0.25	1.71 $\pm$ 0.15	0.91 $\pm$ 0.82	6.37 $\pm$ 0.76	6.11 $\pm$ 0.86	3.06 $\pm$ 0.30
12 + log (S/H)	6.35 $\pm$ 0.05	6.23 $\pm$ 0.04	5.96 $\pm$ 0.04	6.80 $\pm$ 0.05	6.79 $\pm$ 0.06	6.49 $\pm$ 0.04
S/O (x 10 $^2$ )	2.82 $\pm$ 0.44	3.28 $\pm$ 0.36	3.21 $\pm$ 0.35	4.14 $\pm$ 0.53	4.38 $\pm$ 0.70	3.35 $\pm$ 0.44
log (S/O)	-1.55 $\pm$ 0.06	-1.48 $\pm$ 0.04	-1.49 $\pm$ 0.05	-1.38 $\pm$ 0.05	-1.36 $\pm$ 0.06	-1.47 $\pm$ 0.05

Table 3. Comparison of Direct and Empirical Oxygen Abundances

HII Region	Direct	$\log(R_{23})$	$\log(O32)$	M91	P00
ESO 347-G17 #5	$7.90 \pm 0.09$	$0.920 \pm 0.007$	$-0.010 \pm 0.015$	$8.25 \pm 0.05$	$8.22 \pm 0.02$
ESO 347-G17 #10	...	$0.927 \pm 0.008$	$0.242 \pm 0.022$	$8.35 \pm 0.10$	$8.04 \pm 0.02$
ESO 348-G09 #3	...	$0.649 \pm 0.015$	$-0.287 \pm 0.025$	$7.89 \pm 0.03$	$8.11 \pm 0.05$
ESO 471-G06 #2	$7.72 \pm 0.03$	$0.746 \pm 0.006$	$0.228 \pm 0.017$	$7.83 \pm 0.02$	$7.78 \pm 0.02$
ESO 473-G24 #2	$7.45 \pm 0.03$	$0.620 \pm 0.005$	$0.441 \pm 0.018$	$7.60 \pm 0.02$	$7.48 \pm 0.02$
ESO 473-G24 #4	...	$0.549 \pm 0.009$	$0.325 \pm 0.028$	$7.54 \pm 0.02$	$7.44 \pm 0.03$
NGC 625 #5	$8.19 \pm 0.02$	$0.893 \pm 0.003$	$0.537 \pm 0.016$	$8.00 \pm 0.02$	$7.84 \pm 0.01$
NGC 625 #9	$8.14 \pm 0.03$	$0.796 \pm 0.006$	$0.231 \pm 0.016$	$7.92 \pm 0.02$	$7.85 \pm 0.02$
NGC 625 #18	$7.96 \pm 0.04$	$0.832 \pm 0.008$	$0.010 \pm 0.040$	$8.08 \pm 0.03$	$8.08 \pm 0.02$
NGC 625 #21	...	$0.794 \pm 0.032$	$-0.554 \pm 0.042$	$8.31 \pm 0.10$	$8.65 \pm 0.10$

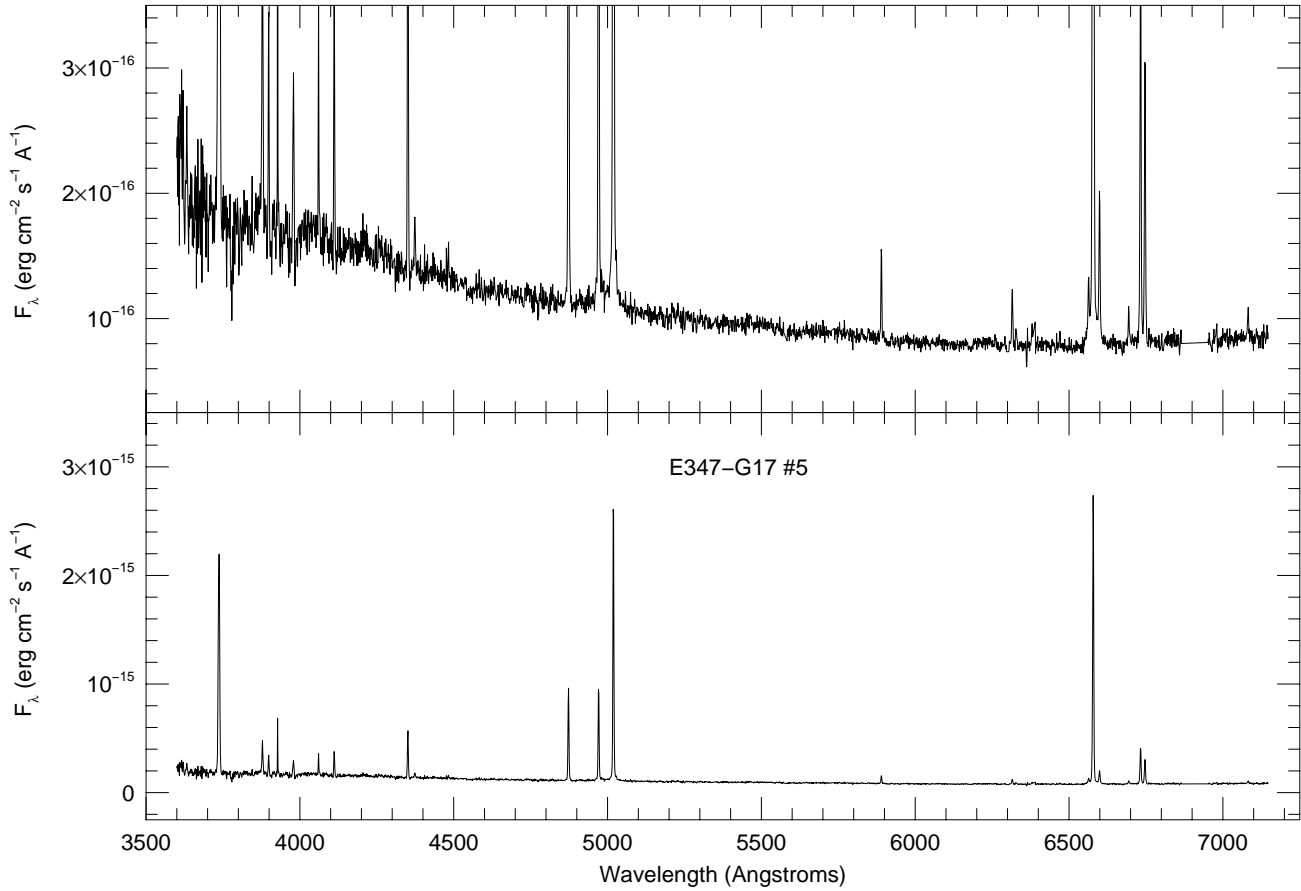
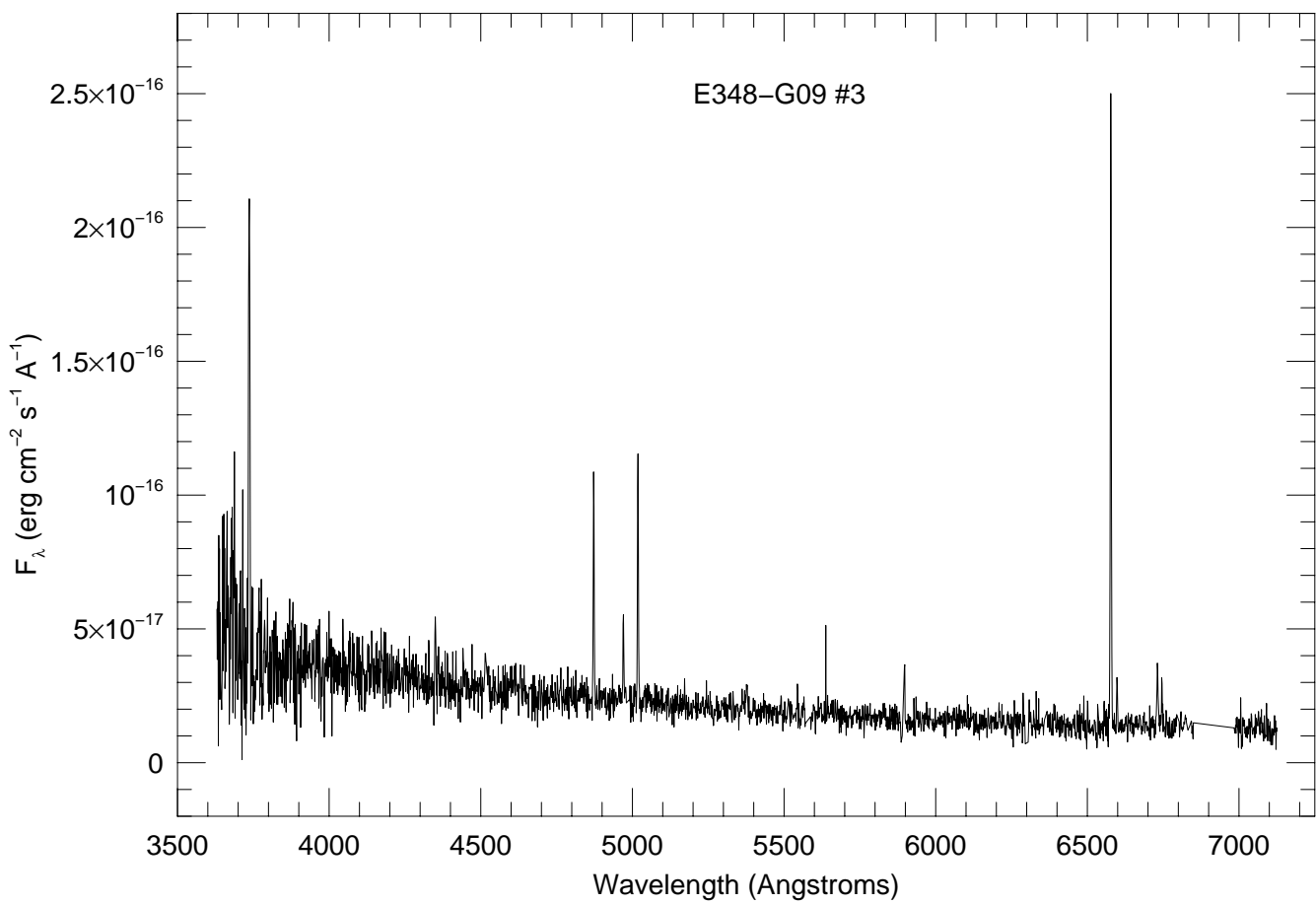
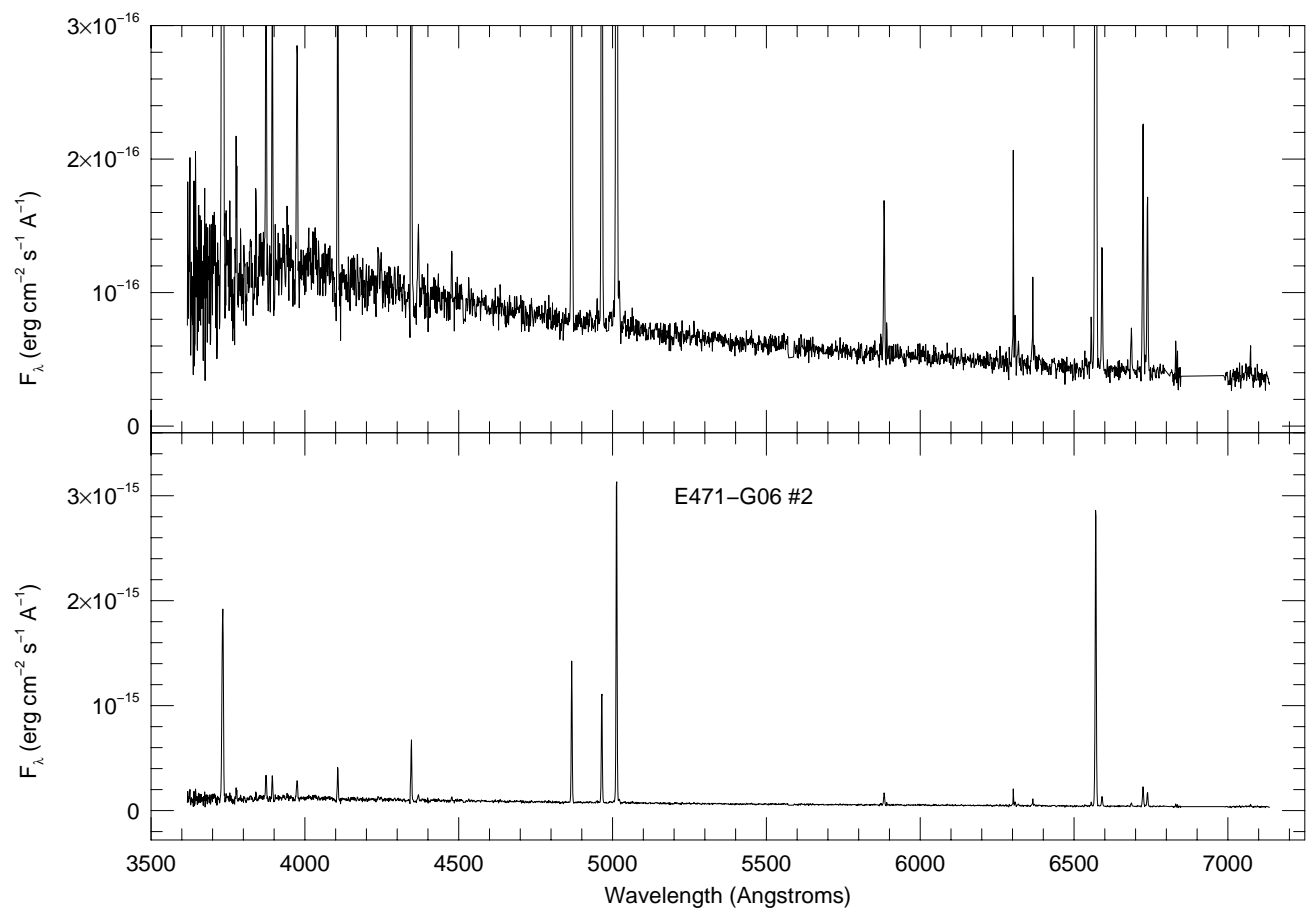
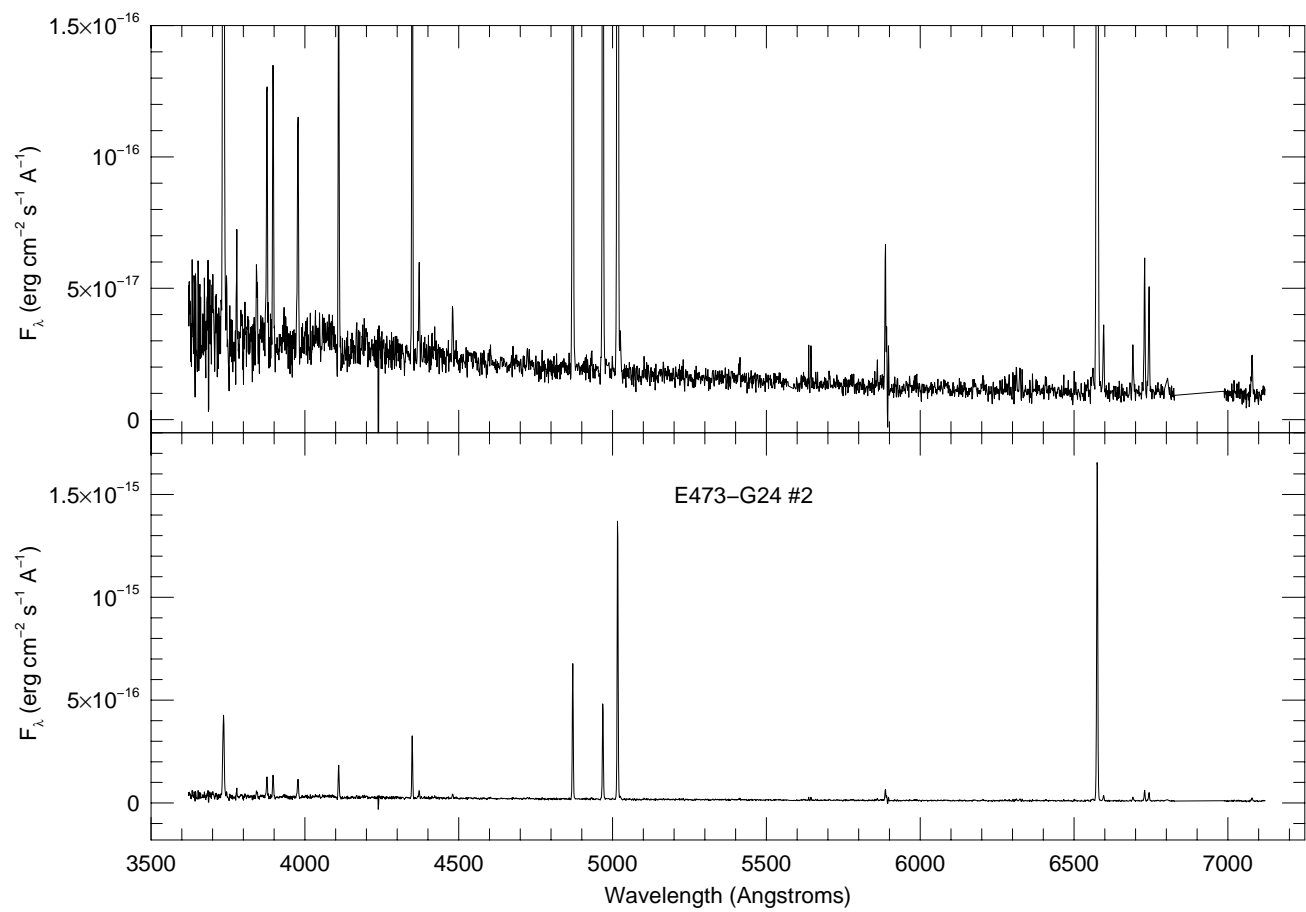
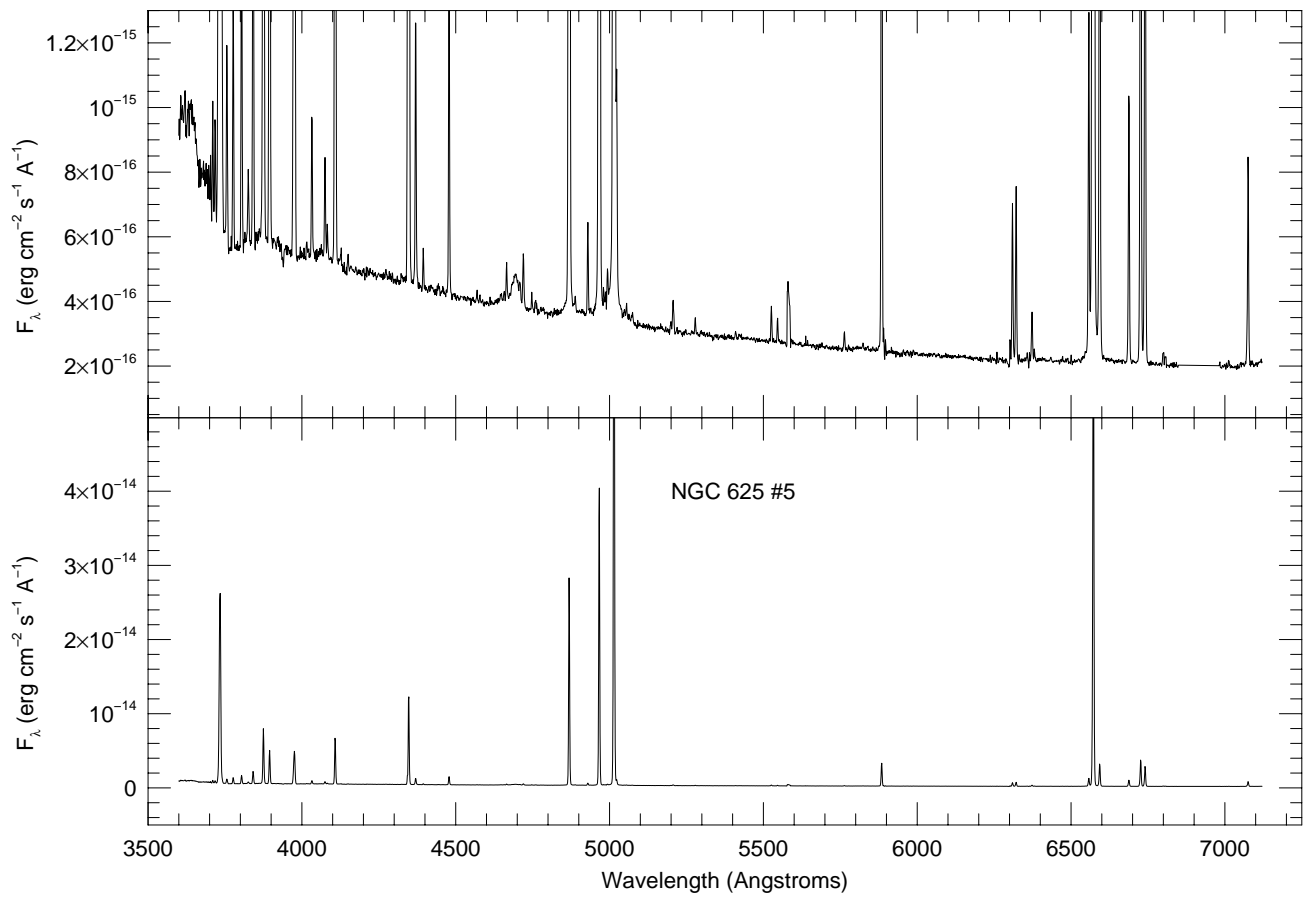


Fig. 1.— Spectra of the brightest HII regions in each of the five Sculptor Group dwarf irregular galaxies observed. For four of the spectra, the upper panel shows a greatly expanded scale in order to show the faintest lines clearly.









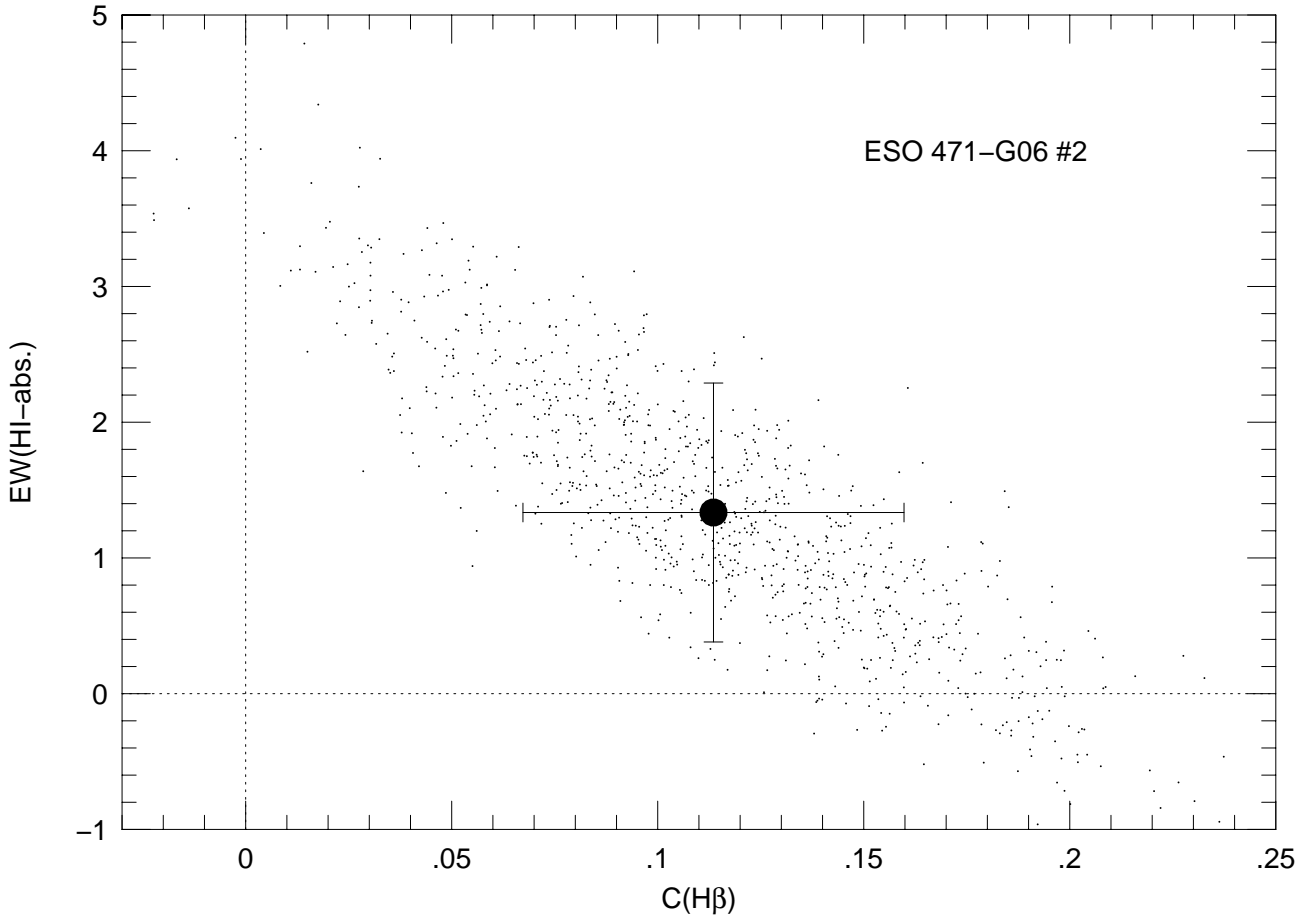


Fig. 2.— The results of Monte Carlo simulations of solutions for the reddening,  $\text{CH}\beta$ , and underlying absorption,  $\text{EW}(\text{HI-abs.})$  from hydrogen Balmer emission line ratios for ESO 471-G05 # 2. Each small point is the solution derived from a different realization of the same input spectrum and errors as given in Table 1. The large filled point with error bars shows the mean result with  $1\sigma$  errors derived from the dispersion in the solutions. Note that the covariance of the two parameters leads to error ellipses. Because of the covariance, the error bars appropriate to these solutions are about twice the size of the errors inferred from a single  $\chi^2$  minimization.

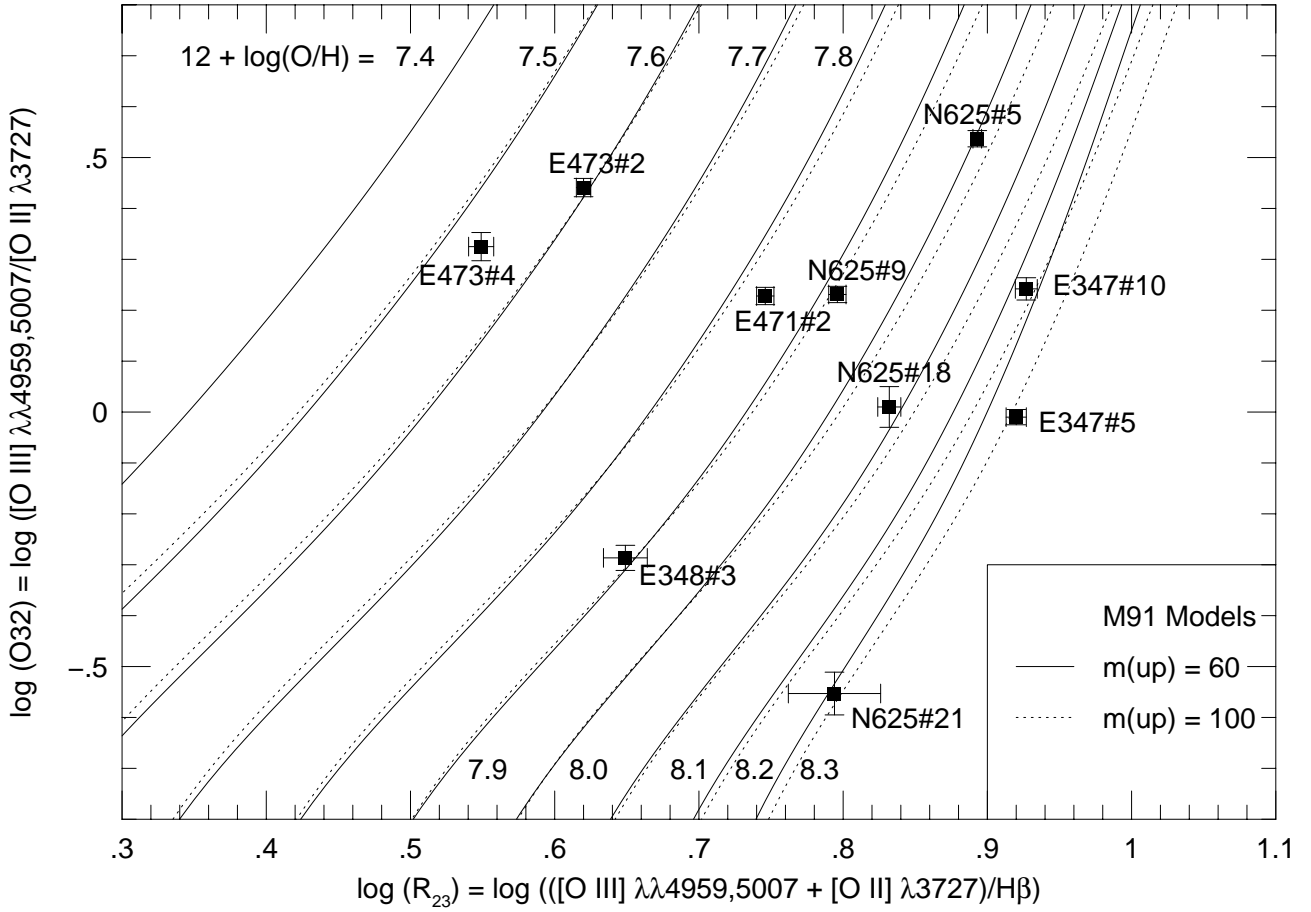


Fig. 3.— Diagnostic diagram of oxygen emission line ratios comparing observed quantities with the photoionization model grid of McGaugh (1991). The two different sets of McGaugh (1991) models correspond to upper limits on the IMF of  $60 M_{\odot}$  and  $100 M_{\odot}$ , and emphasizes his point that there is not a great difference between the two. The results for all ten spectra from Tables 1a - 1c are presented here. Oxygen abundances derived from the McGaugh models are given in Table 3. See text and next two figures for a comparison of oxygen abundances.

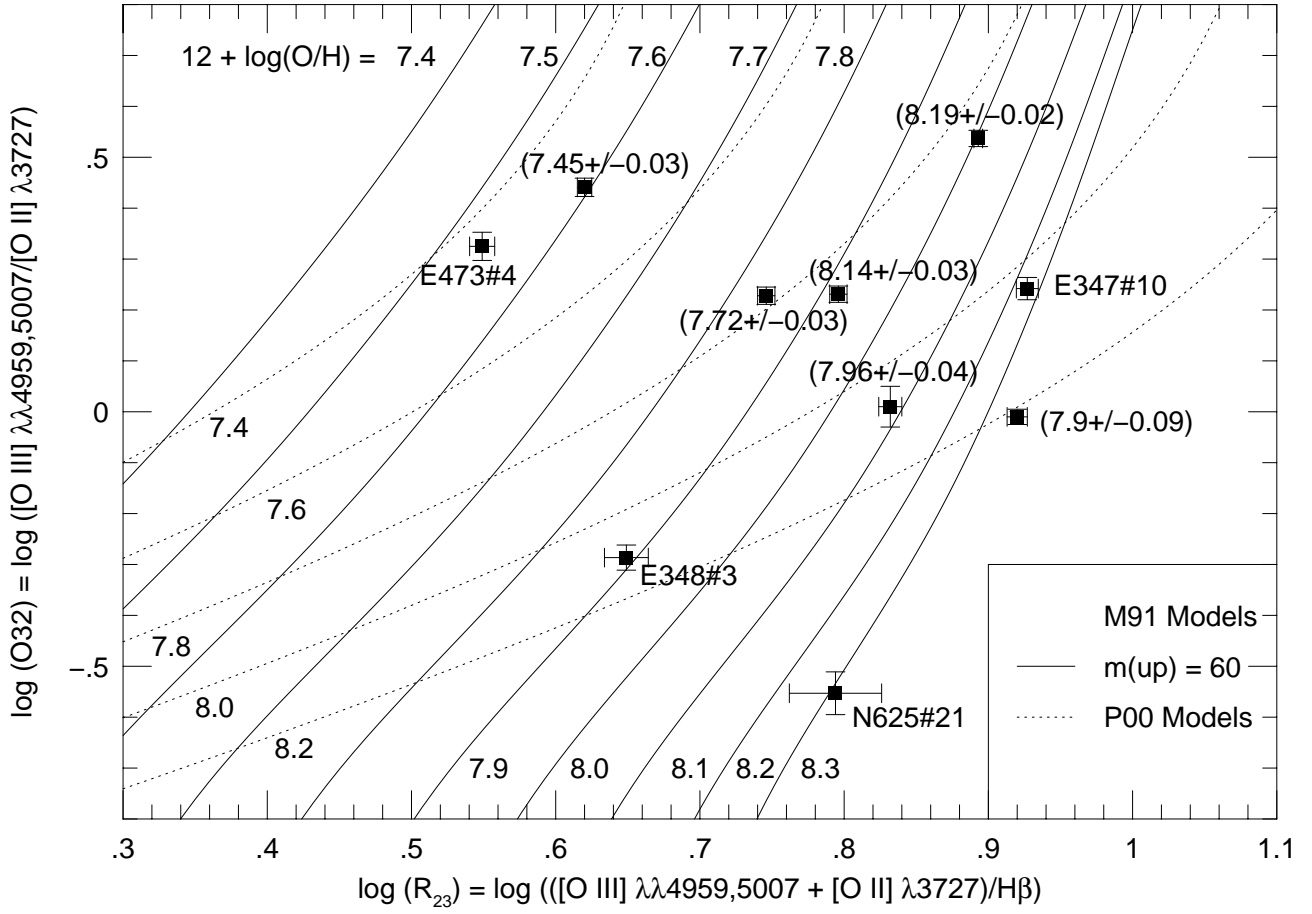


Fig. 4.— Diagnostic diagram of oxygen emission line ratios as in Figure 3, but comparing the observed quantities with both the photoionization models of McGaugh (1991) and the empirical abundances derived via the Pilyugin (2000) method. For those HII regions where  $[O\text{ III}]\lambda 4363$  has been observed, the result of the oxygen abundance derived via the direct method is given as a label.

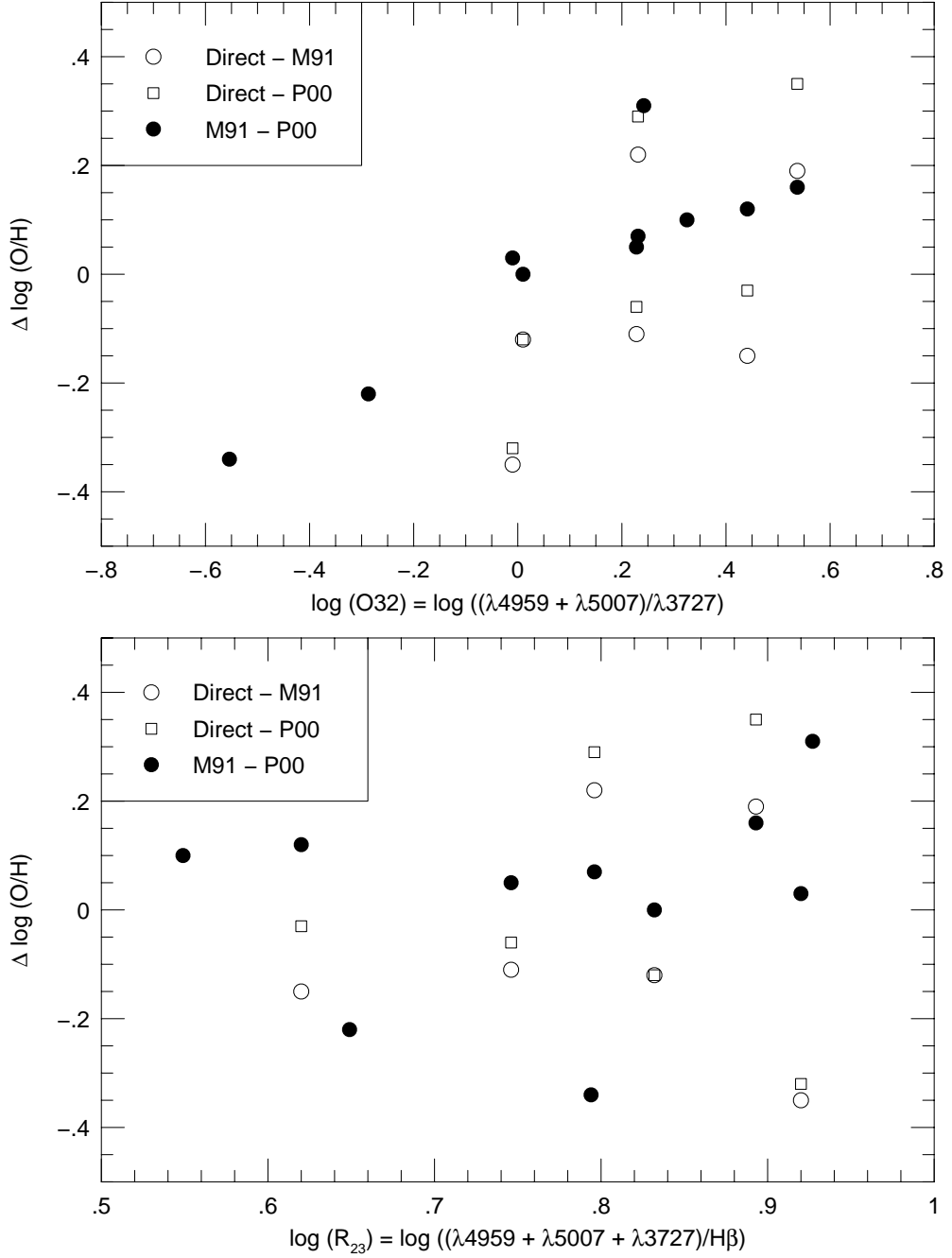


Fig. 5.— Plots of the differences in oxygen abundances derived via three different methods: “Direct” means that an electron temperature derived from the [O III]  $\lambda 4363/(\lambda 4959 + \lambda 5007)$  ratio has been used, M91 means that the grids of McGaugh (1991) has been used, and P00 means that the calibration of Pilyugin (2000) has been used. The differences have been plotted versus  $\log (O32)$  and  $\log (R_{23})$ . In the plot of  $\Delta \log (O/H)$  versus  $\log (O32)$  there is a strong trend in the difference between the calibrations of McGaugh (1991) and Pilyugin (2000).

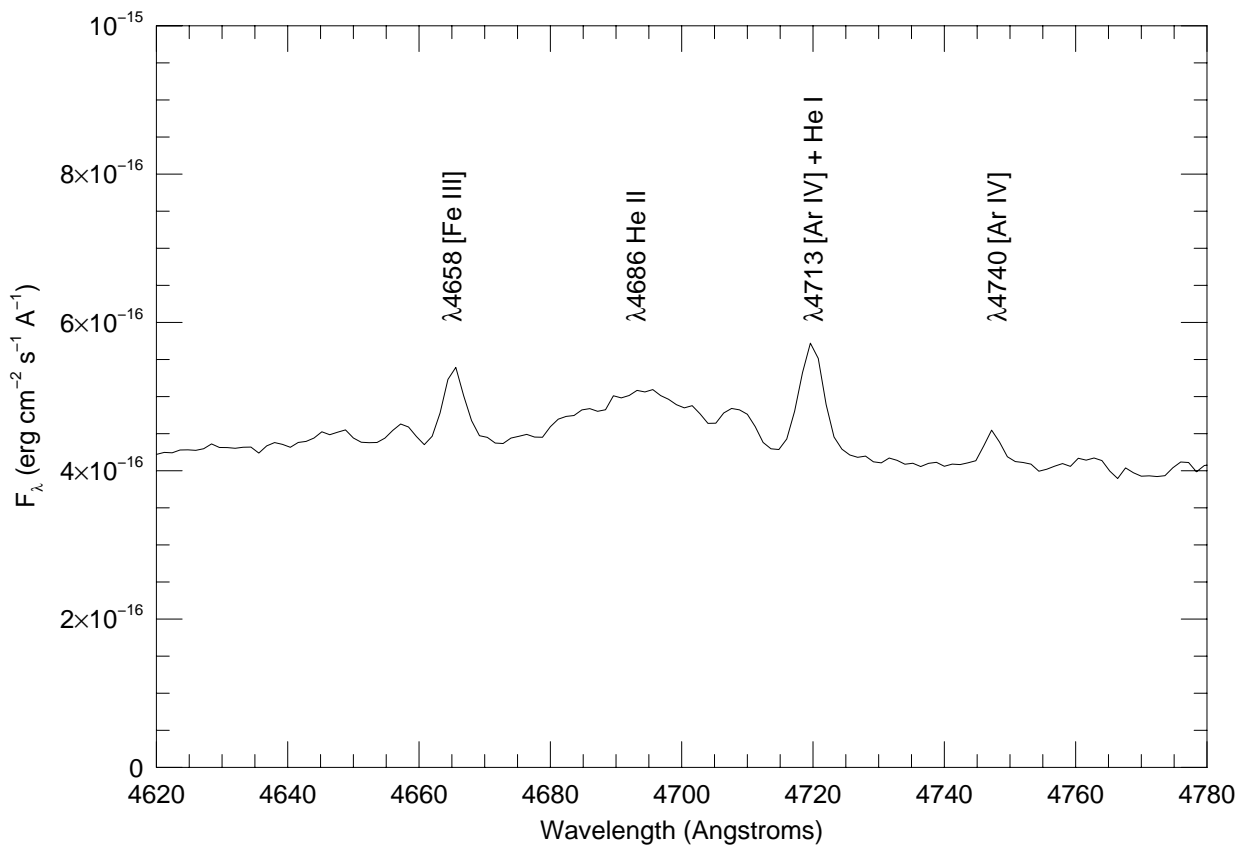


Fig. 6.— Spectrum of NGC 625 #5 in the region of  $\sim \lambda 4700$  where the broad emission of He II is observed.

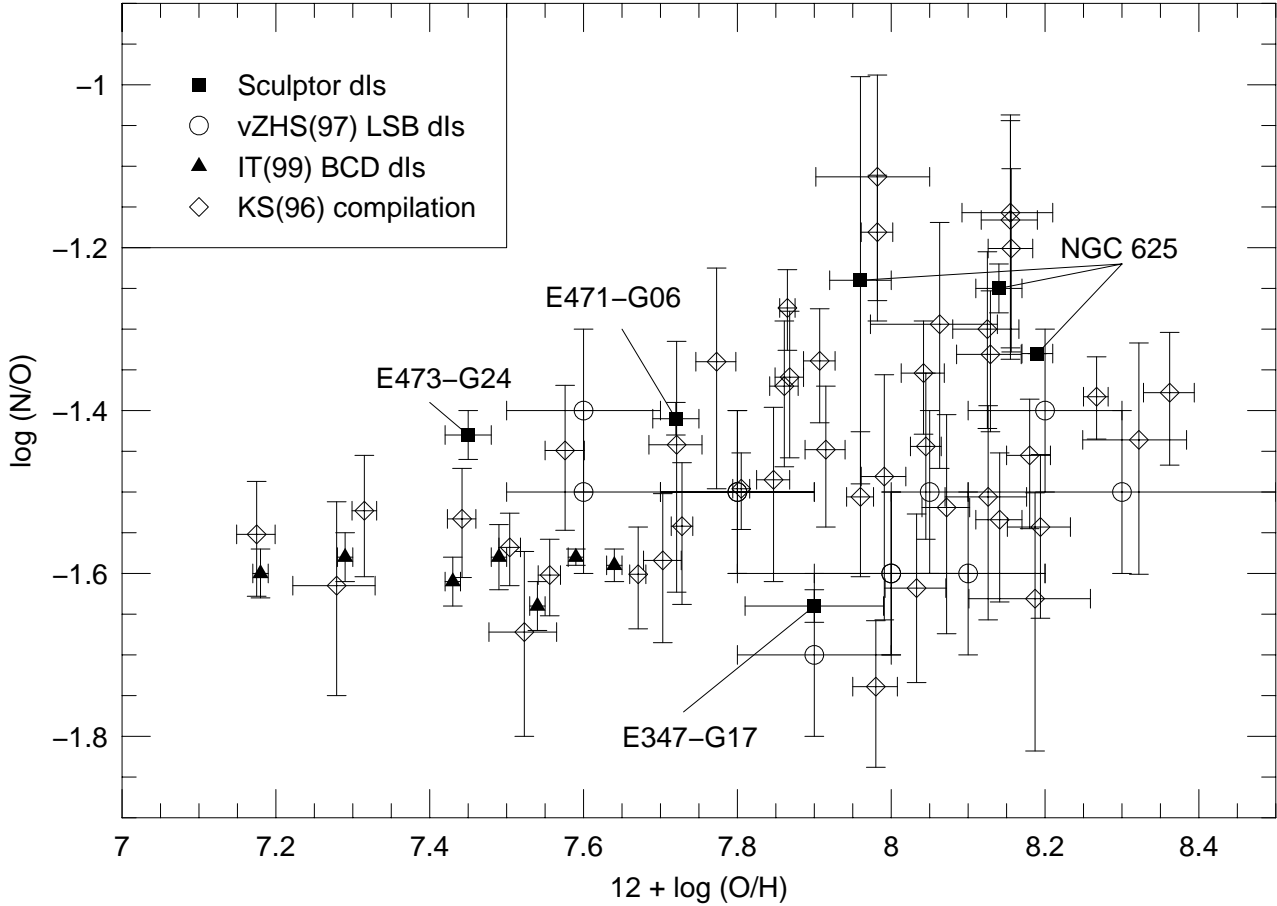


Fig. 7.— A comparison of the N/O and O/H in the Sculptor dwarf irregular galaxies with other star forming dwarf galaxies from the literature. The collection of dwarf irregular galaxies and H II galaxies assembled by Kobulnicky & Skillman (1996; see their Table 5 and Figure 15 for identification of individual points) are represented by open diamonds. Only galaxies without WR emission features and errors in  $\log (\text{N/O})$  less than 0.2 have been plotted. The empty circular symbols represent data for low surface brightness dwarf irregular galaxies from van Zee et al. 1997a. The filled triangles represent the low metallicity blue compact dwarf galaxies from Izotov & Thuan (1999). The four Sculptor dwarf irregular galaxies with direct abundance measurements are shown with filled squares (from the data presented in Table 2).

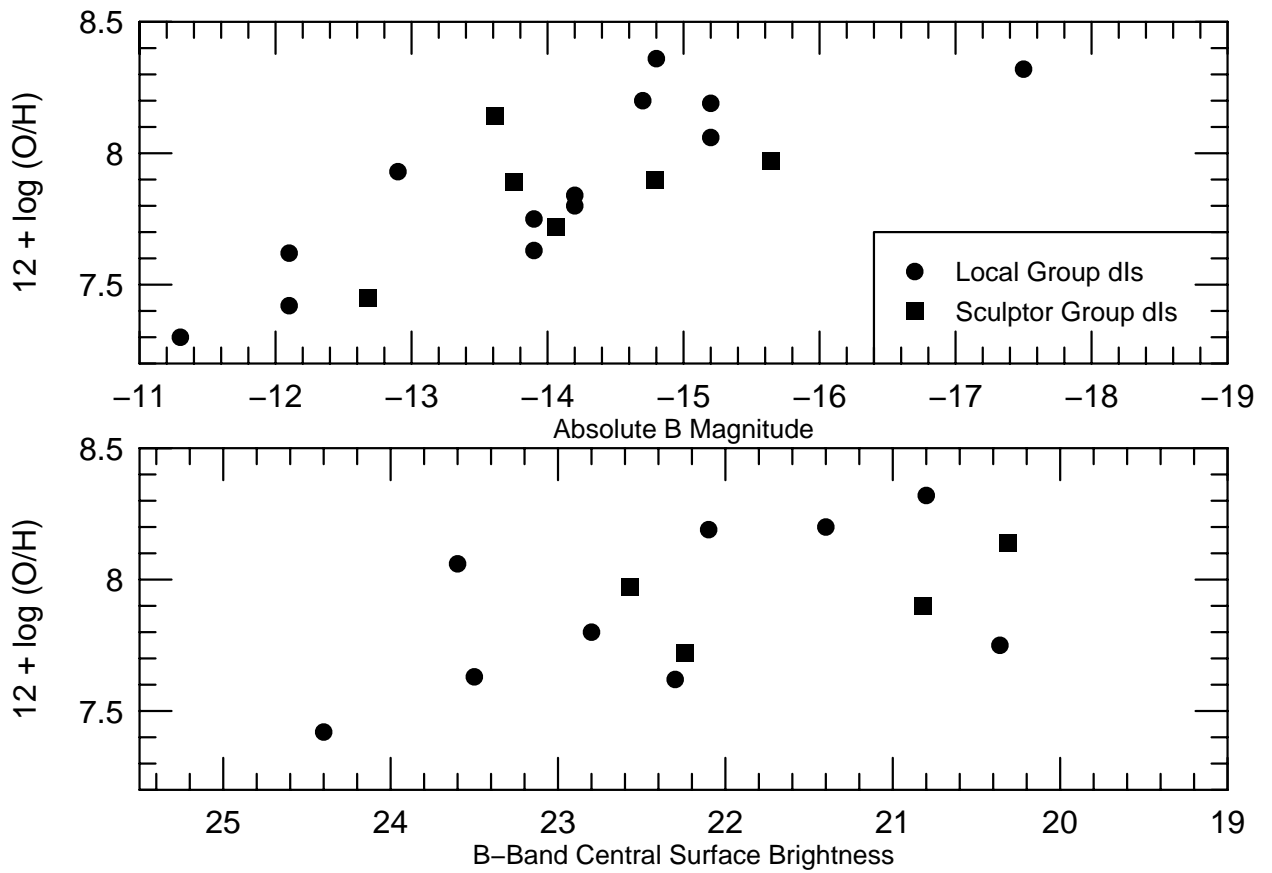


Fig. 8.— Comparison of HII region oxygen abundance versus absolute magnitude and central surface brightness for the Sculptor Group dwarf irregular galaxies with the Local Group dwarf irregular galaxies from the compilation of Mateo (1998).

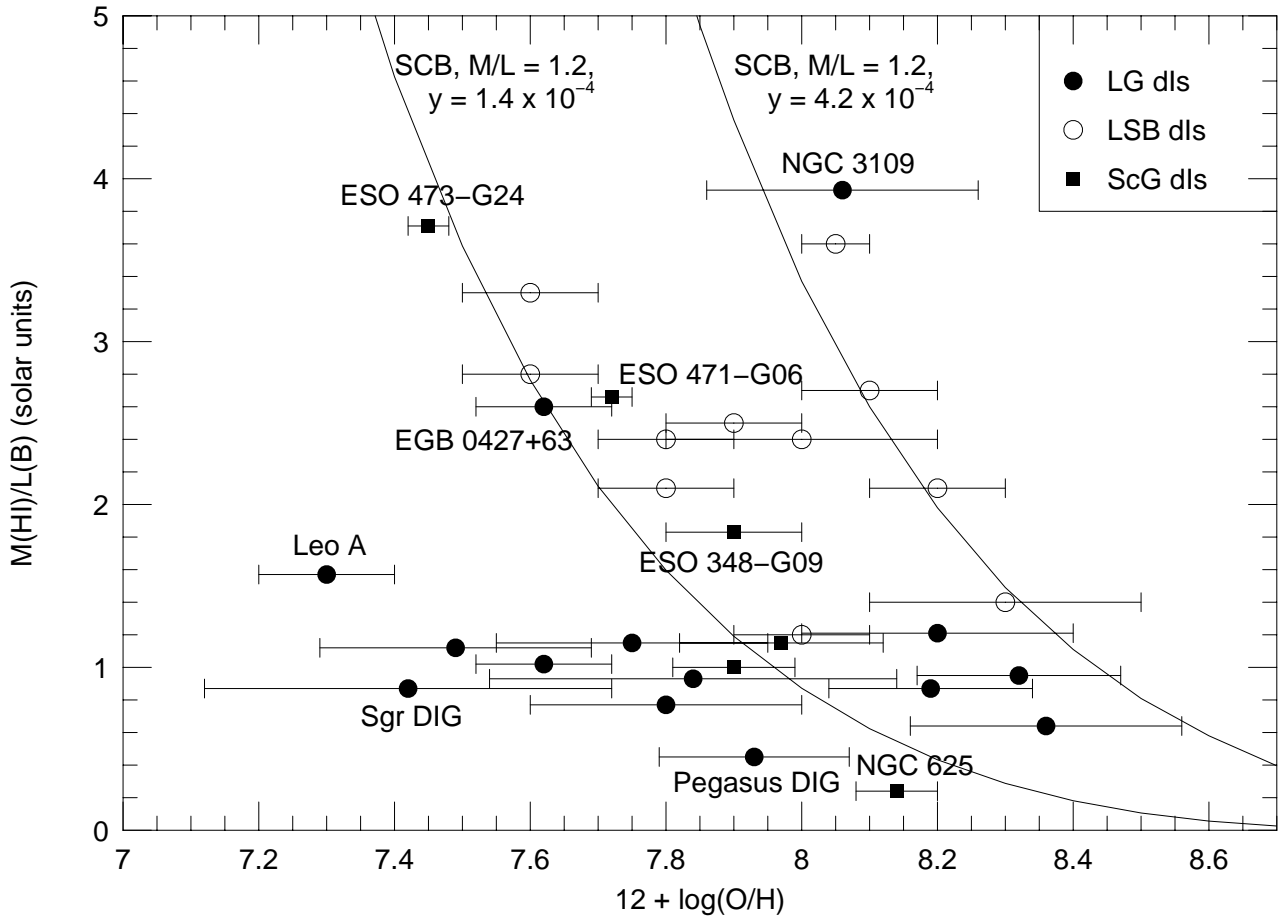


Fig. 9.— Comparison of  $M(\text{HI})/L(\text{B})$  versus  $\log(\text{O/H})$  for the Sculptor Group dwarf irregular galaxies with the Local Group dwarf irregular galaxies from the compilation of Mateo (1998) and LSB dwarf irregular galaxies from van Zee et al. (1997b). The solid curved lines represent the evolution of simple closed box models with the stated parameters. The higher yield curve resulted from a fit to DDO 154 (Kennicutt & Skillman 2001) and is in good agreement with theoretically predicted O yields.